

# Evolution of electron distribution driven by nonlinear resonances with intense field-aligned chorus waves

D. Vainchtein<sup>1,4</sup>, X.-J. Zhang<sup>2,3</sup>, A. V. Artemyev<sup>2,4</sup>, D. Mourenas<sup>5</sup>,

V. Angelopoulos<sup>2</sup>, R. M. Thorne<sup>3</sup>

---

Vainchtein D., Nyheim Plasma Institute, Drexel University, Camden, NJ, USA  
(dlv36@drexel.edu)

Zhang X.-J., Department of Earth, Planetary, and Space Sciences, University of California,  
Los Angeles, USA (xjzhang@ucla.edu)

Artemyev A. V., Department of Earth, Planetary, and Space Sciences, University of California,  
Los Angeles, USA (aartemyev@igpp.ucla.edu)

Mourenas D., CEA, DAM, DIF, F 91297 Arpajon Cedex, France

Angelopoulos V., Department of Earth, Planetary, and Space Sciences, University of California,  
Los Angeles, USA

Thorne R. M., Department of Atmospheric and Oceanic Sciences, University of California, Los  
Angeles, USA

<sup>1</sup>Nyheim Plasma Institute, Drexel  
University, Camden, NJ, USA

<sup>2</sup>Department of Earth, Planetary, and  
Space Sciences, University of California, Los  
Angeles, CA, USA

**Abstract.** Resonant electron interaction with whistler-mode chorus waves is recognized as one of the main drivers of radiation belt dynamics. For moderate wave intensity, this interaction is well described by quasi-linear theory. However, recent statistics of parallel propagating chorus waves have demonstrated that 5 – 20% of the observed waves are sufficiently intense to interact nonlinearly with electrons. Such interactions include phase trapping and phase bunching (nonlinear scattering) effects not described by the quasi-linear diffusion. For sufficiently long (large) wave-packets, these nonlinear effects can result in very rapid electron acceleration and scattering. In this paper we introduce a method to include trapping and nonlinear scattering into the kinetic equation describing the evolution of the electron distribution function. We use statistics of Van Allen Probes and Time History of Events and Macroscale Interactions during Substorms (THEMIS) observations to determine the probability distribution of intense, long wave-packets as function of power and frequency. Then we develop an analytical model of par-

---

<sup>3</sup>Department of Atmospheric and Oceanic Sciences, University of California, Los Angeles, CA, USA

<sup>4</sup>Space Research Institute, Russian Academy of Sciences, Moscow, Russia

<sup>5</sup>CEA, DAM, DIF, Arpajon, France

ticle resonance of an individual particle with an intense chorus wave-packet and derive the main properties of this interaction: probability of electron trapping, energy change due to trapping and nonlinear scattering. These properties are combined in a nonlocal operator acting on the electron distribution function. When multiple waves are present, we average the obtained operator over the observed distributions of waves and examine solutions of the resultant kinetic equation. We also examine energy conservation and its implications in systems with the nonlinear wave-particle interaction.

**Key Points:**

1. *We propose a model of electron nonlinear resonant interaction with long and intense chorus wave-packets*
2. *We derive a new generalized kinetic equation for electrons that encompasses nonlinear interactions with long chorus wave-packets*
3. *Nonlinear interactions with long wave-packets can produce rapid electron acceleration for observed wave characteristics*

**1. Introduction**

The dynamics of Earth’s radiation belts is partly controlled by efficient resonant interactions of electrons with whistler-mode waves [Andronov and Trakhtengerts, 1964; Kennel and Petschek, 1966]. Different modes of these waves are responsible for warm electron precipitation and aurora formation [lower and upper bands chorus waves, see, e.g., Thorne et al., 2010; Ni et al., 2016; Kasahara et al., 2018], electron acceleration and formation of relativistic electron fluxes in the heart of the outer radiation belt [lower band chorus waves, see, e.g., Thorne et al., 2013; Reeves et al., 2013; Li et al., 2014], electron scattering and flux reduction during radial diffusion [hiss waves, see, e.g., Ma et al., 2016; Mourenas et al., 2017], electron scattering in the inner radiation belt [VLF waves from ground-based transmitters, see, e.g., Subbotin et al., 2011; Agapitov et al., 2014b; Ma et al., 2017a]. Depending on their actual characteristics, such whistler-mode waves can resonantly interact with electrons over a wide range of energies starting from 100 eV [very oblique chorus waves, see, e.g., Agapitov et al., 2015b; Artemyev et al., 2015a] and up to several MeVs [intense parallel propagating chorus waves, see, e.g., Omura et al.,

2007]. The wave frequency and obliquity define electron resonant energies [see *Shklyar and Matsumoto*, 2009; *Artemyev et al.*, 2016, and references therein] and the wave intensity determines the regime of resonant interaction. Low intensity waves provide electron diffusive scattering, traditionally described by quasi-linear theory [*Vedenov et al.*, 1962; *Kennel and Engelmann*, 1966]. In the inhomogeneous geomagnetic field of the radiation belts, the applicability of quasi-linear theory can be justified even for narrow band waves [e.g., *Karpman*, 1974; *Karpman and Shklyar*, 1977; *Albert*, 2010] and it has been used to successfully describe many observed phenomena [e.g., *Thorne et al.*, 2013; *Su et al.*, 2014; *Glauert et al.*, 2014; *Ma et al.*, 2015; *Drozdov et al.*, 2015; *Li et al.*, 2016; *Albert et al.*, 2016].

Unlike low intensity waves whose effects on particles have been modeled successfully by diffusion, the consequences of interaction of particles with intense whistler-mode waves for the dynamics of the radiation belts have not yet been fully investigated. There is a common understanding that the generation of intense whistler-mode waves is controlled by nonlinear wave-particle interaction [see reviews *Shklyar and Matsumoto*, 2009; *Omura et al.*, 2013, and references therein], including electron trapping into resonance and a significant modification of the resonant electron distribution function [*Nunn*, 1974; *Karpman et al.*, 1974]. The theory of nonlinear wave generation reproduces many observed properties of intense whistler-mode waves really well [e.g., *Omura et al.*, 2008; *Katoh and Omura*, 2007; *Demekhov*, 2011; *Demekhov et al.*, 2017; *Tao et al.*, 2017; *Shklyar*, 2017]. However, the exact role played by the most intense whistler-mode waves in electron acceleration still remains somewhat controversial. Electron trapping [*Nunn*, 1971] can provide a very long resonant interaction (over a fraction of the electron bounce period along mag-

netic field line), corresponding to a significant change of particle energy [comparable to the initial particle energy, see *Omura et al.*, 2007; *Summers and Omura*, 2007; *Bortnik et al.*, 2008; *Artemyev et al.*, 2012; *Tao et al.*, 2013; *Agapitov et al.*, 2014a]. However, the effects of trapping should be almost compensated by resonant nonlinear scattering, which provides electron drift in energy space in the opposite direction to trapping acceleration [see *Shklyar*, 2011, and references therein]. Although the fine balance between trapping and nonlinear scattering is expected to ultimately establish a kind of diffusive regime of particle acceleration [see *Shklyar*, 1981; *Solovov and Shklyar*, 1986], the actual time required for establishing such a regime can be very long. Thus, when trapping and nonlinear scattering processes do not exactly balance each other, they can potentially provide a very rapid (compared with quasi-linear diffusion) net acceleration of electrons [e.g., *Demekhov et al.*, 2009; *Nunn and Omura*, 2015; *Hsieh and Omura*, 2017]. Models of such rapid acceleration have been able to explain some observations of fast increase of energetic electron flux [e.g., *Agapitov et al.*, 2015a; *Mozer et al.*, 2016; *Foster et al.*, 2017], but the global importance of such fast acceleration processes in the overall radiation belt dynamics remains unknown.

To include the nonlinear resonant interactions into global models of wave-particle interaction in the radiation belts one needs: (i) representative statistics of intense wave characteristics based on spacecraft measurements and (ii) a universal approach for the description of the evolution of the electron distribution due to nonlinear interactions. There is a lack of information about fine wave characteristics such as the intensity and duration of individual wave-packets. Because most wave statistics are collected for use in quasi-linear diffusion codes, their focus is on the average wave intensity, over long time intervals

[see, e.g., *Meredith et al.*, 2012; *Li et al.*, 2013; *Agapitov et al.*, 2013]. Such averaging mixes two different wave populations, low intensity waves and transient bursts of high intensity waves, and it does not allow to consider them separately afterwards. Thus, most wave statistics do not contain any information about wave-packet characteristics, such as the duration of wave-packets (or wave-packet modulation), which are critical for modeling nonlinear wave-particle interaction [*Tao et al.*, 2012, 2013; *Artemyev et al.*, 2012] but not important for quasi-linear models. Recently, *Zhang et al.* [2018] analyzed THEMIS and Van Allen Probe measurements of intense parallel chorus whistler-mode waves and identified the portion of the wave population that may potentially interact with electrons in the nonlinear regime. Most of intense chorus waves ( $\sim 95 - 99\%$ ) were found to propagate in the form of short wave-packets, allowing resonant interaction with electrons over only a very short time, despite their large intensity [*Zhang et al.*, 2018; *Mourenas et al.*, 2018]. Only a few the intense waves propagate in the form of long wave-packets and can efficiently accelerate trapped electrons. In this study we use the statistics collected by *Zhang et al.* [2018] to quantify how these few percents of intense wave-packets that are sufficiently long to produce a significant nonlinear acceleration affect the electron distribution.

Although the test particle approach provides a satisfactory description of the effects of the nonlinear resonant interactions on the electron distribution [*Bortnik et al.*, 2008; *Yoon et al.*, 2013; *Nunn and Omura*, 2015; *Agapitov et al.*, 2016], this approach cannot be used to calculate the long-term dynamics of the radiation belts. Therefore, theoretical estimates of electron acceleration/deceleration due to nonlinear trapping and scattering [e.g., *Shklyar*, 1981; *Bell*, 1984; *Albert*, 1993] should be combined in some operator acting on the full electron distribution function to complement and generalize the usual quasi-

linear diffusion equation. Several examples of such operators were developed numerically [e.g., *Omura et al.*, 2015; *Hsieh and Omura*, 2017] and analytically in the two opposite limiting cases of infinitely long wave-packets [e.g., *Artemyev et al.*, 2014a, 2016] and short wave-packets [*Mourenas et al.*, 2018]. However, for long but finite wave-packets, one should consider realistic distributions of intense wave characteristics. Nonlinear operators describing fast particle transport in energy space due to trapping contain nonlocal terms describing transport between different distant energy/pitch-angle domains (see schematic in Fig. 1). Averaging such nonlocal operators over the distribution of observed wave characteristics is therefore a difficult, still unsolved problem.

In this study, we attempt to quantify the effects of the nonlinear wave-particle interaction on the evolution of the global electron distribution. First we use statistics of intense, long wave-packet chorus waves collected by *Zhang et al.* [2018] to determine their probability distribution as function of wave intensity and frequency (Sect. 2). Then we consider the nonlinear wave-particle interaction and determine its main characteristics (Sect. 3). These characteristics are used to construct a generalized kinetic equation including the effects of nonlinear wave-particle interactions with long wave-packets (Sect. 4). The operators of this equation are averaged over the observed distribution of wave characteristics. Then, we demonstrate how the averaged nonlinear effects drive the evolution of the electron distribution (Sect. 5). Finally, we discuss the applicability of the proposed approach for the description of the actual dynamics of the radiation belts and the particular constraints on the electron distribution that follow from the obtained solutions of the generalized kinetic equation (Sect. 6).



## 2. Intense whistler-mode wave characteristics

Two wave characteristics that are the most important for the nonlinear wave-particle interaction are the wave amplitude  $B_w$  (square root of wave intensity) and the duration of the wave-packet, given here by the number  $\beta$  of wave periods within one packet. The normalized wave amplitude is  $\mathcal{B}_w = R\Omega_{ce}B_w/cB_0$ , where  $B_0$  is the equatorial background magnetic field,  $\Omega_{ce}$  the equatorial electron gyrofrequency,  $R = R_E L$  the spatial scale of the background magnetic field inhomogeneity, and  $c$  the speed of light. If  $\mathcal{B}_w > 2$ , nonlinear interaction is possible, while for  $\mathcal{B}_w < 1 - 2$  the wave is not sufficiently intense to trap particles [for more details, see *Zhang et al.*, 2018; *Mourenas et al.*, 2018, and references therein]. A more precise evaluation of the critical wave amplitude necessary for the nonlinear interaction depends on additional wave characteristics (e.g., frequency drift) and resonant particle energy and pitch-angle [see, e.g., *Karpman*, 1974; *Bell*, 1986; *Le Queau and Roux*, 1987], but a aforementioned simplified  $\mathcal{B}_w$ -criteria is sufficiently accurate to process the observed wave statistics and provide first-order estimates of the impact on the electron distribution. We use lower-band chorus wave statistics collected by *Zhang et al.* [2018] for  $\mathcal{B}_w > 2$ . Five years of THEMIS [*Angelopoulos*, 2008] and three years of Van Allen Probes [*Mauk et al.*, 2013] wave measurements have been analyzed to identify intense chorus wave-packets and determine their characteristics. Onboard THEMIS, wave fields are measured by search coil magnetometers [*Le Contel et al.*, 2008] and the electric field instrument [*Bonnell et al.*, 2008]. We also use measurements of three components of the background magnetic field by the fluxgate magnetometer [*Auster et al.*, 2008]. The two identical Van Allen Probes measure electric and magnetic field waveforms using the Electric Fields and Waves [*Wygant et al.*, 2013] and the Electric and Magnetic

Field Instrument Suite and Integrated Science [*Kletzing et al.*, 2013] detectors. The data is transmitted at 35000 samples/s over 6s intervals in burst mode.

Due to the difference between THEMIS and Van Allen Probe operational modes (the absolute majority of the THEMIS waveforms measurements are triggered by plasma injections), the occurrence rate of  $\mathcal{B}_w > 2$  waves are different for datasets collected by THEMIS and the Van Allen Probes, but on average there are  $< 1\%$  of intense ( $\mathcal{B}_w > 2$ ) parallel chorus waves propagating along magnetic field lines in the form of long wave-packets (with  $\beta \geq 50$ ). One example of a long wave-packet is shown in Figure 2. The main wave parameters,  $B_w$  and frequency  $\omega$ , are defined for each such packet and normalized on the background characteristics:  $B_w/B_0$  and  $\omega/\Omega_{ce}$  where  $B_0$  and  $\Omega_{ce}$  are evaluated using the equatorial geomagnetic field. Because most of THEMIS and Van Allen Probe measurements are not equatorial, we use  $L^*$  for Van Allen Probe data to approximate the equatorial field and  $B_z$  GSM measurements of THEMIS (at large  $L$ -shell) as a proxy of the equatorial field. All THEMIS measurements are restricted to the near-equatorial region with  $B_z > \sqrt{B_x^2 + B_y^2}$ .

The number of chorus wave-packets with  $\mathcal{B}_w > 2$  and  $\beta > 50$  captured by THEMIS and the Van Allen Probes per day of intense chorus wave measurements are shown in Fig. 3(a) as a function of  $L$ -shell. Van Allen Probes ( $L < 6$ ) captured much more wave-packets than THEMIS ( $L > 6$ ), but the occurrence rate of intense waves is larger at larger  $L$  (where THEMIS spacecraft provide most of the statistics). This is mainly due to the shorter total time of waveform measurements by THEMIS [see details in *Zhang et al.*, 2018]. The parameter  $\beta^*$  is number of wave-periods with wave magnetic field larger than half of the peak wave-packet magnetic field. The distribution of the number of observed wave-packets

with  $\beta^* > 50$  (dotted lines in Fig. 3(a)) shows that packets with  $\beta^* > 50$  represent only  $\sim 15 - 20\%$  of all long wave-packets with  $\beta > 50$ . The remaining  $\sim 80 - 85\%$  of these long wave-packets are actually still very localized, i.e., most of the wave intensity is located near the position of peak intensity, while the remaining part (the tails) of the wave-packet is much less intense. This factor can be important for realistic estimates of the efficiency of nonlinear wave-particle interaction in the radiation belts.

We separate the  $L^*$ -shell range into two intervals: (1) the outer radiation belt with  $L^*$  between the plasmasphere [as defined by the model from *O'Brien and Moldwin, 2003*] and the geostationary orbit  $L^* \sim 6.6$ , and (2) the injection region at  $L^* \in [6.6, 9]$ . These two  $L^*$ -shell ranges roughly separate Van Allen Probe measurements (outer radiation belt) and THEMIS measurements (injection region). For both  $L^*$ -shell ranges, we plot the wave-packet distributions in the  $(B_w/B_0, \omega/\Omega_{ce})$  space. Figures 3(b) and (c) show the presence of a significant portion of intense ( $B_w/B_0 \in [10^{-3}, 10^{-2}]$ ) waves with  $\omega/\Omega_{ce} \in [0.2, 0.4]$ . We use these wave distributions to estimate the average effect of the nonlinear wave-particle interaction on the evolution of the electron distribution.

### 3. Nonlinear resonances

We consider a simple planar magnetic field model [*Bell, 1984*] with a single vector potential component  $A_{0y} = -xB_0(z)$ , where  $z$  is a field-aligned coordinate and  $B_0(z)$  mimics the dipolar geomagnetic field ( $B_0 = \sqrt{1 + 3 \sin^2 \lambda} / \cos^6 \lambda$  where  $dz/d\lambda = R\sqrt{1 + 3 \sin^2 \lambda}$  and  $R = R_E L$ ). The parallel propagating whistler-mode wave is described by two components of the vector potential:  $A_x = (B_w/k) \sin \phi$  and  $A_y = (B_w/k) \cos \phi$  where  $B_w$  and  $k$  are the wave amplitude and wave vector ( $B_w$  and  $k$  depend on  $z/R$ ), and  $\phi$  is the wave phase ( $\partial\phi/\partial z = k$ ,  $\partial\phi/\partial t = -\omega$ ). The Hamiltonian of a relativistic electron (the charge

being  $-e$  and the rest mass  $m_e$ ) in such electromagnetic fields is

$$H = \sqrt{m_e^2 c^4 + c^2 p_z^2 + (c p_x + e A_x)^2} + e^2 (A_{0y} + A_y)^2 \quad (1)$$

We expand Hamiltonian (1) over a small parameter  $eB_w/km_e c^2 \ll 1$  and introduce new conjugate variables, the gyrophase  $\psi$  and magnetic moment  $I_x = \oint p_x dx$  [see details of Hamiltonian transformation in, e.g., *Artemyev et al.*, 2015c, 2018]. The new Hamiltonian takes the form:

$$H = m_e c^2 \gamma + U_w(z, I_x) \sin(\phi + \psi), \quad \gamma = \sqrt{1 + \frac{p_z^2}{m_e^2 c^2} + \frac{2I_x \Omega_{ce}}{m_e c^2}} \quad (2)$$

where  $\gamma$  is the gamma factor of the gyro-averaged system,  $\Omega_{ce} = eB_0(z)/m_e c$ , and  $U_w = \sqrt{2I_x \Omega_{ce}} e B_w / \gamma m_e c k$  is the effective wave amplitude. The Hamiltonian equations describe electron motion:

$$\begin{aligned} \dot{z} &= \frac{\partial H}{\partial p_z} = \frac{p_z}{\gamma m_e} + \frac{\partial U_w}{\partial p_z} \sin(\phi + \psi) \\ \dot{\psi} &= \frac{\partial H}{\partial I_x} = \frac{\Omega_{ce}}{\gamma} + \frac{\partial U_w}{\partial I_x} \sin(\phi + \psi) \\ \dot{p}_z &= -\frac{\partial H}{\partial z} = -\frac{I_x \Omega'_{ce}}{\gamma} - k U_w \cos(\phi + \psi) + \frac{\partial U_w}{\partial z} \sin(\phi + \psi) \\ \dot{I}_x &= -\frac{\partial H}{\partial \psi} = -U_w \cos(\phi + \psi), \quad \dot{\phi} = k \dot{z} - \omega \end{aligned} \quad (3)$$

where  $\Omega'_{ce} = d\Omega_{ce}/dz$ . In the absence of waves ( $U_w = 0$ ), electrons move along the bounce trajectory  $\dot{z} = p_z/\gamma m_e$ ,  $\dot{p}_z = -I_x \Omega'_{ce}/\gamma$  with a constant energy  $\gamma$  and magnetic moment  $I_x$ . Waves disturb these bounce oscillations and can scatter or trap particles (see Fig. 4). For sufficiently intense waves, as considered in this study, nonlinear scattering results in energy change with a finite mean value  $\langle \Delta \gamma \rangle = \Delta \gamma_{scat} \neq 0$  [see details in, e.g., *Solovév and Shklyar*, 1986; *Albert*, 2002]. Energy changes due to trapping and nonlinear scattering significantly exceed the square root of energy variance (see relations between  $\Delta \gamma_{scat}$ ,  $\Delta \gamma_{trap}$  and energy spread in Fig. 4), i.e., trapping and nonlinear scattering are the dominant

processes, whereas energy diffusion is much weaker. The diffusion process likely becomes important on very long time intervals, but it can be omitted over relatively short intervals (still including many resonant interactions). Therefore, we focus here on the description of trapping and nonlinear scattering of electrons and on the effects of these processes on the evolution of the full electron distribution function.

Three main characteristics define the resonant interaction: (i) the probability of trapping,  $\Pi$ , gives the relative number of resonant particles trapped during one resonant interaction (the relative number of scattered particles is equal to  $1 - \Pi$ ); (ii) the energy change due to trapping  $\Delta\gamma_{trap}$ ; (iii) the energy change due to nonlinear scattering  $\Delta\gamma_{scat}$ . These characteristics depend on the initial particle energy  $\gamma$  and on the initial value of  $I_x$ .  $I_x$  can be written through the energy and equatorial pitch-angle  $\alpha_{eq}$  as  $I_x = m_e c^2 (\gamma^2 - 1) \sin^2 \alpha_{eq} / 2\Omega_{ce}(0)$ . Thus, we use the notation  $\Pi(\gamma, \alpha_{eq})$ ,  $\Delta\gamma_{scat}(\gamma, \alpha_{eq})$ ,  $\Delta\gamma_{trap}(\gamma, \alpha_{eq})$ . These characteristics can be combined to construct a nonlocal (integral) operator acting on the full electron distribution function to describe its evolution due to the nonlinear wave-particle interaction [e.g., *Solovev and Shkliar, 1986; Artemyev et al., 2016; Omura et al., 2015*].

The probability of trapping,  $\Pi$ , can be obtained numerically using Hamiltonian equations (3). We bin  $(\gamma, \alpha_{eq})$  space, and for each  $(\gamma, \alpha_{eq})$  we calculated trajectories of  $5 \cdot 10^3$  particles with the same initial position  $z = 0$  and different randomly distributed phases  $\psi$  (initial  $p_z$  and  $I_x$  are defined by  $(\gamma, \alpha_{eq})$ ). Each trajectory is integrated for a half of the bounce period. The final  $(\gamma, \alpha_{eq})$  determines whether this particle was trapped (increase of  $\Delta\gamma$  exceeding 10% of the initial  $\gamma$ ) or scattered ( $\Delta\gamma < 0$ ). The relative number of trapped particles is shown in Fig. 5(a) for one particular set of system parameters (see the figure

caption). Although such a calculation of  $\Pi$  is relatively straightforward, it requires a lot of test particles with sufficiently small bins in  $(\gamma, \alpha_{eq})$  space. Such a procedure should be repeated for all sets of the system parameters (wave amplitudes, wave frequencies, etc.). Thus a purely numerical determination of  $\Pi$  is not very effective. Alternatively,  $\Pi$  can be obtained analytically [e.g., *Neishtadt, 1975; Shklyar, 1981; Neishtadt et al., 1989*]. We use here the approach developed in *Artemyev et al. [2015c]* (see details of  $\Pi$  calculations in Appendix A, Eq. (21)). We plotted  $\Pi(\gamma, \alpha_{eq})$  in Figs. 5(a,b). Figure 5(a) demonstrates that the analytical equations describe  $\Pi$  well. Thus, we shall use the analytically derived distribution  $\Pi(\gamma, \alpha_{eq})$  (like the one shown in Fig. 5(b)) to describe the trapping probability for the construction of a nonlocal operator acting on the full distribution function.

The coordinates of particle resonant interaction with the wave in the  $(z, p_z)$  plane are defined by the resonant condition  $\dot{\phi} + \dot{\psi} = 0$  and the unperturbed particle trajectory ( $\gamma = const, I_x = const$ ). There is an additional condition for trapping, which can be formulated in a simplified form as a requirement of growth of the ratio of the wave force acting on the resonant particle over the combined mirror and inertial forces [see more accurate definition in, e.g., *Neishtadt, 1975; Neishtadt et al., 2011*]. Particles trapped at some  $z_{trap}$  escape from the resonance at  $z_{esc}$ . The energy change is  $\Delta\gamma_{trap} = \gamma_R(z_{esc}) - \gamma_R(z_{trap})$ , where energy  $\gamma_R$  along the resonant trajectory is defined as (see Eq. (16) in Appendix A and [e.g., *Artemyev et al., 2018*])

$$\gamma_R = \left| \varpi \mp \frac{N}{\sqrt{N^2 - 1}} \sqrt{1 - 2\varepsilon_0\varpi + \varpi^2} \right| \quad (4)$$

In Eq. (4),  $\varpi = \Omega_{ce}(z)/\omega$ ,  $N = k(z)c/\omega$ , and  $\varepsilon_0 = \gamma - \omega(\gamma^2 - 1) \sin^2 \alpha_{eq}/2\Omega_{ce}(0) = const$ . The sign in Eq. (4) is defined by the sign of the resonant velocity  $\sim (1 - \varpi/\gamma)/N$ . For a simple cyclotron resonance with  $\varpi/\gamma > 1$  and negative resonant velocity  $\sim (1 -$

$\varpi/\gamma)/N < 0$ , Eq. (4) should be used with a ‘-’, while for the turning acceleration with  $\varpi/\gamma < 1$  and  $(1 - \varpi/\gamma)/N > 0$  [Omura *et al.*, 2007], Eq. (4) should be used with a ‘+’. To estimate  $\Delta\gamma_{trap}$ , we have to determine  $z_{esc}$ . The condition of particle escape from the resonance is determined by particle motion in the  $(\zeta, \dot{\zeta})$  phase plane, where  $\zeta = \phi + \psi$ . The computation of  $z_{esc}$  and  $\Delta\gamma_{trap}$  is described in Appendix B. The obtained analytical expression for  $\Delta\gamma_{trap}$  can be tested using numerical integration of the Hamiltonian equations (3). Figure 5(c) compares numerical and analytical distributions  $\Delta\gamma_{trap}(\gamma, \alpha_{eq})$ . We also indicate the energy gain due to the turning acceleration, when the direction of trapped particles motion changes and the particles gain significantly more energy than through an usual cyclotron resonance [see details in Omura *et al.*, 2007]. This comparison shows that we can use the analytical distributions from Fig. 5(d) to characterize electron trapping acceleration.

To complete the description, we need the energy change  $\Delta\gamma_{scat}$ . As nonlinear scattering is a local process,  $\Delta\gamma_{scat}$  depends on wave properties and background magnetic field characteristics at the resonant location in the  $(z, p_z)$  plane:  $\Delta\gamma_{scat} = -\omega S_{res}/2\pi$  where

$$S_{res} = \sqrt{\frac{8r}{g}} \int_{\zeta_-}^{\zeta_+} \sqrt{a(\sin \zeta_+ - \sin \zeta) - (\zeta_+ - \zeta)} d\zeta \quad (5)$$

$g = \omega^2(N^2 - 1)/m_e^2 c^4 \gamma_R$ , and  $r = r(z)$ ,  $a = a(z)$  (see Appendix C and [e.g., Artemyev *et al.*, 2014b]). The integration limits,  $\zeta_{\pm}$ , are defined in Eq. (20) in Appendix C. The resonance location depends on the initial  $(\gamma, \alpha_{eq})$  and thus we can define  $\Delta\gamma_{scat}(\gamma, \alpha_{eq})$ . To check the analytical  $\Delta\gamma_{scat}(\gamma, \alpha_{eq})$ , we used the same approach as we used for II. We bin  $(\gamma, \alpha_{eq})$  space and for each pair of  $\gamma, \alpha_{eq}$  values we numerically integrated  $5 \cdot 10^3$  trajectories of test particles. Then we calculated the energy change after a single resonant interaction for each particle and averaged these changes over the non-trapped (scattered)

particles. Figure 5(e) shows  $\Delta\gamma_{scat}(\gamma, \alpha_{eq})$  obtained from the numerical integration of particle trajectories, and the analytically evaluated  $\Delta\gamma_{scat}(\gamma, \alpha_{eq})$ . This comparison confirms that we can use the analytical distributions  $\Delta\gamma_{scat}(\gamma, \alpha_{eq})$  from Fig. 5(f) to describe the dynamics of an ensemble of charged particles.

## 4. Kinetic equation

### 4.1. Single wave

The nonlinear trapping and scattering of resonant electrons results in evolution of the electron distribution function  $\Psi(\gamma, \alpha_{eq})$ . To describe this evolution, we need a generalized kinetic equation that includes effects of nonlinear scattering [i.e., drift in energy space, see, e.g., *Albert, 2002*] and trapping [i.e., fast transport in energy space, e.g., see *Omura et al., 2007*]. Let us start with a system with one wave frequency,  $\omega$ . The particle energy in the wave reference frame is an integral of motion [e.g., *Summers et al., 1998*, and references therein]. Using the resonant condition  $\dot{\phi} + \dot{\psi} = 0$  (i.e.,  $kp_z - \gamma\omega + \Omega_{ce} = 0$ ), this integral can be written as  $m_e c^2 \gamma - \omega I_x = const$  (alternatively,  $\gamma - (\omega/2\Omega_{ce}(0)) (\gamma^2 - 1) \sin^2 \alpha_{eq} = const$ ). Thus, for systems with one  $\omega$ , the energy change directly defines the pitch-angle change

$$\Delta\alpha_{eq} = \Delta\gamma \frac{\Omega_{ce}(0) - \omega\gamma \sin^2 \alpha_{eq}}{\omega (\gamma^2 - 1) \sin \alpha_{eq} \cos \alpha_{eq}} \quad (6)$$

This relation allows to compute  $\Delta\alpha_{scat}$ ,  $\Delta\alpha_{trap}$  once  $\Delta\gamma_{scat}$ ,  $\Delta\gamma_{trap}$  are known. The relation between  $\gamma$  and  $\alpha_{eq}$  can be used to examine the evolution of the 1D distribution function  $\Psi(\gamma, \varepsilon_0)$  where  $\varepsilon_0 = \gamma - (\omega/2\Omega_{ce}(0)) (\gamma^2 - 1) \sin^2 \alpha_{eq}$  is a constant parameter. The kinetic equation describing the evolution of a particle distribution has been derived in *Artemyev et al. [2018]*. However, this kinetic equation does not allow a simple averaging over wave characteristics ( $\omega$ ,  $B_w$ , etc.). Therefore, we follow the approach proposed by *Omura et al.*



[2015], and use  $\Pi$ ,  $\Delta\gamma_{trap}$ ,  $\Delta\gamma_{scat}$  to derive the operator acting on  $\Psi$ . Note that in contrast to *Omura et al.* [2015], we use here analytical expressions for  $\Pi$ ,  $\Delta\gamma_{trap}$ , and  $\Delta\gamma_{scat}$ .

We bin the  $(\gamma, \alpha_{eq})$  space as  $\gamma^{(i)} = 1 + \Delta\gamma i$ ,  $\alpha_{eq}^{(j)} = \Delta\alpha j$  where  $i, j = 0 \dots M$  and  $\Delta\alpha = \pi/M$ ,  $\Delta\gamma = (\gamma_{\max} - 1)/M$ . Then for each bin  $(\gamma^{(i)}, \alpha_{eq}^{(j)})$ , we define  $\Pi^{ij}$ ,  $\Delta\gamma_{scat}^{ij}$ ,  $\Delta\gamma_{trap}^{ij}$ , and introduce two quantities:  $s_{mn}^{kl}(W)$  and  $p_{mn}^{kl}(W)$  denoting the probabilities for a particle to move from the state  $(\gamma^{(k)}, \alpha_{eq}^{(l)})$  to the state  $(\gamma^{(m)}, \alpha_{eq}^{(n)})$  due to a single nonlinear scattering ( $s_{mn}^{kl}$ ) and trapping ( $p_{mn}^{kl}$ ). The letter  $W$  indicates all the relevant wave-packet characteristics, most importantly its amplitude  $B_w$  and frequency  $\omega$ . For each packet (fixed  $B_w$ ,  $\omega$ ), one can view all  $s_{mn}^{kl}(W)$ ,  $p_{mn}^{kl}(W)$  as the elements of a big 4D matrix that defines the phase space transport due to scattering and trapping. Both  $s_{mn}^{kl}(W)$  and  $p_{mn}^{kl}(W)$  are obtained using  $\Pi^{ij}$ ,  $\Delta\gamma_{trap}^{ij}$ , and  $\Delta\gamma_{scat}^{ij}$ :

$$s_{mn}^{kl} = \begin{cases} 1 - \Pi^{kl}, & \gamma^{(k)} + \Delta\gamma_{scat}^{kl} \in \left[ \gamma^{(m)} - \frac{\Delta\gamma}{2}, \gamma^{(m)} + \frac{\Delta\gamma}{2} \right] \\ & \alpha_{eq}^{(l)} + \Delta\alpha_{eq,scat}^{kl} \in \left[ \alpha_{eq}^{(n)} - \frac{\Delta\alpha}{2}, \alpha_{eq}^{(n)} + \frac{\Delta\alpha}{2} \right] \\ 0, & \text{otherwise} \end{cases} \quad (7)$$

$$p_{mn}^{kl} = \begin{cases} \Pi^{kl}, & \gamma^{(k)} + \Delta\gamma_{trap}^{kl} \in \left[ \gamma^{(m)} - \frac{\Delta\gamma}{2}, \gamma^{(m)} + \frac{\Delta\gamma}{2} \right] \\ & \alpha_{eq}^{(l)} + \Delta\alpha_{eq,trap}^{kl} \in \left[ \alpha_{eq}^{(n)} - \frac{\Delta\alpha}{2}, \alpha_{eq}^{(n)} + \frac{\Delta\alpha}{2} \right] \\ 0, & \text{otherwise} \end{cases}$$

Consider a state  $(\gamma^{(i)}, \alpha_{eq}^{(j)})$ . During each bounce period  $\tau_{ij} = \tau(\gamma^{(i)}, \alpha_{eq}^{(j)})$ , a particle undergoes  $n_{ij} = n(\gamma^{(i)}, \alpha_{eq}^{(j)})$  resonant interactions. Combining nonlinear scattering and trapping, we obtain a joint evolution equation of the electron distribution in the case of a single wave:

$$\frac{\partial \Psi_{ij}}{\partial t} = -\frac{n_{ij}}{\tau_{ij}} \Psi_{ij} + \sum_{kl} \frac{n_{kl}}{\tau_{kl}} s_{ij}^{kl}(W) \Psi_{kl} + \sum_{kl} \frac{n_{kl}}{\tau_{kl}} p_{ij}^{kl}(W) \Psi_{kl} \quad (8)$$

where  $\Psi_{ij} = \Psi(\gamma^{(i)}, \alpha_{eq}^{(j)})$ . The summation is performed over a set of indices  $(k, l)$  for which  $s_{ij}^{kl}$  or  $p_{ij}^{kl}$  is non-zero – in other words, over all the states  $(\gamma^{(k)}, \alpha_{eq}^{(l)})$  from which particles can come to the state  $(\gamma^{(i)}, \alpha_{eq}^{(j)})$  after a single nonlinear scattering or trapping, as shown

in Fig. 6. The negative term proportional to  $\Psi_{ij}$  describes the removal of particles from the state  $(\gamma^{(i)}, \alpha_{eq}^{(j)})$ , while the terms with the sum describe the incoming flux of particles. There is a noticeable difference between  $s_{mn}^{kl}(W)$  and  $p_{mn}^{kl}(W)$ : while the non-null elements of  $s_{mn}^{kl}(W)$  correspond to nearby cells (around  $k = m, l = n$ ), the elements of  $p_{mn}^{kl}(W)$  are more remote, see Fig. 6.

Equation (8) can be rewritten as

$$\begin{aligned} \frac{\partial \Psi_{ij}}{\partial t} &= -\frac{n_{ij}}{\tau_{ij}} \Psi_{ij} + \sum_{kl} R_{ij}^{kl}(W) \Psi_{kl} \\ R_{ij}^{kl}(W) &= \frac{n_{kl}}{\tau_{kl}} \left( s_{ij}^{kl}(W) + p_{ij}^{kl}(W) \right) \end{aligned} \quad (9)$$

Elements of  $R_{ij}^{kl}(W)$  depend on wave characteristics. Note that Eq.(9) is linear with respect to  $\Psi_{ij}$  and all the nonlinearity is included in  $R_{ij}^{kl}(W)$ . Equation (9) fully defines the evolution of  $\Psi_{ij}$  in the presence of a single wave (i.e., for a given  $W$ ). To generalize the results obtained to an ensemble of waves, we need to average Eq. (9) weighted by the probability (occurrence rate) of the different wave parameters (different sets of  $W$ ).

## 4.2. Multiple waves

Consider an ensemble of waves, where  $\rho(W)$  defines the normalized statistical weight of a certain set of parameters (e.g., each of the two probability distributions in Fig. 3 could result in an empirical determination of  $\rho(W)$  as function of wave amplitude  $B_w$  and frequency  $\omega$ ). Here, however, the distribution  $\rho(W)$  is normalized so that  $\int \rho(W) dW = T_{int}/T_{tot}$ , where  $T_{tot}$  is the total time interval of spacecraft wave measurements and  $T_{int}$  is the cumulative time interval of observations of intense ( $\mathcal{B}_w > 2$ ) and long chorus wave-packets. Instead of Eq. (9), we obtain

$$\frac{\partial \Psi_{ij}}{\partial t} = \int_W \left( -\frac{n_{ij}}{\tau_{ij}} \Psi_{ij} + \sum_{kl} R_{ij}^{kl}(W) \Psi_{kl} \right) \rho(W) dW \quad (10)$$

As  $\Psi_{ij}$  does not explicitly depend on the wave properties  $W$ , it can be taken out of the integral. Moreover, in the first approximation (for relatively narrow-band parallel chorus waves interacting with electrons through the single fundamental cyclotron resonance),  $n_{ij}$  and  $\tau_{ij}$  are roughly independent of  $W$ . Thus we get

$$\begin{aligned} \frac{\partial \Psi_{ij}}{\partial t} &= -\frac{n_{ij}}{\tau_{ij}} \frac{T_{int}}{T_{tot}} \Psi_{ij} + \left( \int_W \sum_{kl} R_{ij}^{kl}(W) \rho(W) dW \right) \Psi_{kl} \\ &= -\frac{n_{ij}}{\tau_{ij}} \frac{T_{int}}{T_{tot}} \Psi_{ij} + \sum_{kl} \langle R_{ij}^{kl} \rangle \Psi_{kl} \end{aligned} \quad (11)$$

where  $\langle R_{ij}^{kl} \rangle = \int_W R_{ij}^{kl}(W) \rho(W) dW$ . Typical plots of  $\rho(W)$  and  $\langle R_{ij}^{kl} \rangle$  are shown in Fig. 7. For the first-order cyclotron resonance, nonlinear scattering results in energy/pitch-angle decrease and trapping results in energy/pitch-angle increase. Therefore, for a given state  $(\gamma^{(i)}, \alpha_{eq}^{(j)})$ , the matrix  $\langle R_{ij}^{kl} \rangle$  contains two groups of non-zero elements: (i) elements at energies/pitch-angles slightly larger than the *target* cell describe the efficiency of nonlinear scattering; (ii) elements located at energies/pitch-angles quite smaller than the *target* cell describe the efficiency of trapping.

## 5. Evolution of the electron distribution

Equation (11) describes the long-term evolution of the electron distribution function due to nonlinear wave-particle interaction. To demonstrate how this theoretical approach works for realistic waves, we parameterize the distribution of prolonged and intense chorus waves from Fig. 3b (at  $L^* < 6.6$ ) and substitute it as  $\rho(W)$  into Eq. (11). We use the normalized time  $\tau = t(c/R_E)(T_{int}/T_{tot})$  and thus the  $\rho$  distribution is normalized to unity ( $\int \rho dW = 1$ ). We take  $T_{int}/T_{tot} \approx 10^{-3}$  during active periods with  $AE \geq 500$  nT, in agreement with the chorus wave statistics showing that long wave-packets with  $\beta > 50$  represent  $\sim 2\%$  of intense wave observations, which themselves are present during  $\sim 10\%$

of lower-band chorus wave measurements performed during active periods between 20 MLT and 10 MLT – the MLT range of intense chorus emissions, representing 58% of the full MLT range [see *Zhang et al.*, 2018; *Mourenas et al.*, 2018]. Therefore, normalized time  $\tau = 1$  corresponds to  $\sim 21$  seconds in real time.

Both nonlinear scattering and trapping have a pronounced effect on  $\Psi(\gamma, \alpha_{eq})$  and  $\bar{\Psi}(\gamma)$ . Figure 8 shows  $\Psi(\gamma, \alpha_{eq})$  and  $\bar{\Psi}(\gamma) = \int_0^{\pi/2} \Psi(\gamma, \alpha_{eq}) \sin \alpha_{eq} d\alpha_{eq}$  at  $\tau = 10$  ( $\sim 4$  minutes),  $\tau = 30$  ( $\sim 10$  minutes),  $\tau = 60$  ( $\sim 21$  minutes), and  $\tau = 100$  ( $\sim 35$  minutes) of the nonlinear wave-particle interaction. The main feature of the distribution displayed in Fig. 8 is a heavily reduced middle domain at  $\alpha_{eq} \in [30^\circ, 70^\circ]$  and energies  $\in [10^2, 10^3]$  keV). Electron interaction with an ensemble of intense chorus waves leads to an efficient nonlinear scattering toward smaller energies/pitch-angles ( $\Psi$  increases at energies  $\sim 30$  keV below the domain of reduced phase space density) and trapping acceleration to larger energies ( $\Psi$  increases at energies  $\sim 3$  MeV above the domain of reduced phase space density). Both the decelerated low-energy electron population and the accelerated high-energy population (see peaks in the energy spectra  $\bar{\Psi}(\gamma)$  increasing around 30 keV and 3 MeV in the bottom panels of Fig. 8) are formed after a relatively short time ( $\sim 35$  minutes) when considering the time-averaged characteristics of intense chorus waves from Fig. 3b – in spite of the presence of 30-40 % waves with  $B_w/B_0 < 0.0035$  generally not sufficiently intense to produce NL effects. Moreover, the occurrence rate of long and intense chorus wave-packets can become 3-5 times higher than time-averaged level used. This can occur over short time intervals ( $\sim 10$  minutes) corresponding to plasma injections during dipolarization events at  $L^* \sim 5$  [*Zhang et al.*, 2018]. In principle, this could result in an even faster evolution of  $\Psi$  at low electron energy  $< 100$  keV (corresponding to an

azimuthal drift period  $> 1$  hour), but barely accelerates the evolution of  $\Psi$  at  $0.4 - 3$  MeV because the azimuthal drift period of such electrons is 5-25 minutes, which implies that the particles encounter such rare events (localized in MLT) during only a small fraction of one azimuthal drift period. However, we caution that various other effects can modify the efficiency of nonlinear interaction and that they should be carefully taken into account to estimate the actual time scale of the evolution of the electron distribution. These will be discussed in details in section 6.

Figure 8 demonstrates the presence of both acceleration and deceleration of resonant electrons: nonlinear scattering results in particle drift to smaller energies and trapping transports particles to higher energies. These two processes should be in fine balance due to the strong relation linking the probability of trapping and the scattering drift rate [see, e.g., *Solovév and Shklyar, 1986; Artemyev et al., 2018*]. The analytical theory predicts that the total energy change of resonant electrons should not be large [*Shklyar, 2011*], because any significant energy change necessitates some energy source or sink. Thus if the total energy varies, either the assumption of roughly constant wave intensity is not satisfied or the initial electron distribution was not chosen properly. To check the prediction of small energy change we plotted the average particle energy  $m_e c^2 \langle \gamma - 1 \rangle$  as a function of time for  $\Psi$  from Fig. 8. A weak but still significant (several percent) decrease of  $m_e c^2 \langle \gamma - 1 \rangle$ , indicates that the initial distribution  $\Psi$  may not have been chosen fully properly, Fig. 9(left panel). However, the slope of the initial energy distribution (the  $\kappa$  parameter) does not significantly influence the rate of decrease.

## 6. Discussion

In this study, we focused on the electron nonlinear resonant interactions with long and intense chorus wave-packets which can support a rapid evolution of the electron distribution via trapping and nonlinear scattering. When combined with the previous investigations of electron diffusion by low-intensity waves [see *Schulz and Lanzerotti*, 1974; *Lyons and Williams*, 1984, and references therein] and intense short wave-packets [see *Mourenas et al.*, 2018], the present investigation complements the set of theoretical tools needed to fully describe electron dynamics driven by realistic whistler-mode waves in the radiation belts. Here, we discuss several important questions arising from a careful analysis of solutions of Eq. (11).

### 6.1. Time scale of electron distribution evolution

Figure 8 shows that the typical time scale of the evolution of the electron distribution via nonlinear trapping and scattering by long and intense chorus wave-packets can be about half an hour, i.e., rather short compared with  $\sim 4 - 10$  hours typically for quasi-linear diffusion by the bulk of lower-intensity chorus waves [e.g., *Mourenas et al.*, 2014; *Li et al.*, 2016; *Ma et al.*, 2017b; *Yang et al.*, 2018]. Although such fast electron flux variations have been occasionally observed [e.g., *Agapitov et al.*, 2015a; *Foster et al.*, 2017], they are rather unusual. Therefore, we discuss below the possible effects that can slow down the nonlinear evolution of the electron distribution.

First, during low geomagnetic activity the occurrence rate of intense chorus waves is reduced [see the dependence of intense wave occurrence rate on the  $AE$  index in *Zhang et al.*, 2018]. Accordingly, the characteristic time scale of electron acceleration would be considerably increased as compared with  $AE \geq 500$  nT. Moreover, even during geomag-

netically active periods, intense long wave-packets are observed only sporadically. Time intervals when such long wave-packets are present mainly correspond to intervals ( $\sim 10$  minutes) of significant plasma injections that provide a free energy source for strong wave generation [e.g., *Tao et al.*, 2011; *Demekhov et al.*, 2017; *Zhang et al.*, 2018]. Such realistic chorus wave-packets are limited in time and space [spatial scales of the source region of chorus waves are about  $\sim 500 - 1000$  km, see *Agapitov et al.*, 2017]. Thus, they have a smaller (and slower) effect on the electron distribution than those in Fig. 8, where we considered very long wave-packets present all the time with their time-averaged occurrence rate. Quasi-linear diffusion coefficients can be directly calculated by time-averaging the wave intensity. To obtain the nonlinear resonant operator in Eq. (11) we can average operator over a distribution of long intense wave-packet characteristics and multiple it by the percentage of time when such wave-packets are observed. However, nonlinear effects described by this operator may be significantly smoothed and slowed down (compared with results of Fig. 8), if short periods of really intense wave-packet observations are mixed with long periods of moderately intense waves. This may partly explain why the effects of the nonlinear wave-particle interaction (rapid electron energization/scattering) can be observed mostly within short periods of intense waves. These effects are barely noticeable in the long-term dynamics of the outer radiation belt.

Second, there is an important additional factor that can reduce the efficiency of the nonlinear wave-particle interaction, slowing down the global evolution of the electron distribution. Even long wave-packets may not always sustain a prolonged nonlinear interaction, because of a possible destruction of the nonlinear resonance by adverse effects [caused by additional resonant sidebands of lower amplitude, or non-resonant weaker waves, see

*Nunn*, 1986; *Shklyar and Zimbardo*, 2014; *Artemyev et al.*, 2015b]. The length (and/or amplitude) of long wave-packets should also probably decrease as they propagate toward higher latitudes [*Tsurutani et al.*, 2011]. This effect reduces the rate of trapping acceleration [e.g., *Artemyev et al.*, 2012]. Intense chorus wave statistics presented in Fig. 3 were obtained at low latitudes, inside or near the wave source region. Moreover, Fig. 3(a) indicates that important modulations of the wave intensity are generally present inside long wave-packets, which can result in a further reduction of the efficiency of nonlinear wave-particle interaction [*Tao et al.*, 2013; *Artemyev et al.*, 2015b]. Only  $\sim 15 - 20\%$  of intense long wave-packets (with  $\beta > 50$ ) contain at least  $\sim 50$  wave-periods with a wave amplitude larger than the half of the peak wave-packet amplitude, i.e., most of the long wave-packets are rather localized, with a narrow peak of wave intensity and much less intense *tails*. Based on this last effect alone, the typical time scale of nonlinear evolution of the electron distribution can be increased by a factor  $\sim 5 - 6$  as compared with Fig.8, reaching already 3 – 4 hours, similar to quasi-linear time scales.

## 6.2. Nonlinear wave-particle interaction vs. quasi-linear models

Equation (11) describes changes of the electron distribution  $\Psi$  due to the nonlinear wave-particle interaction. This equation has the form of a classical evolution equation [e.g., *Van Kampen*, 2003]: the time derivative  $\partial\Psi/\partial t$  is equal to an operator  $\hat{L}$  acting on  $\Psi$ :  $\partial\Psi/\partial t = \hat{L}\Psi$ . The same type of equation describes quasi-linear particle diffusion by an ensemble of low-intensity waves,  $\partial\Psi/\partial t = \hat{D}\Psi$  [*Schulz and Lanzerotti*, 1974], where the diffusion operator  $\hat{D} \sim \partial^2/\partial\gamma^2, \partial^2/\partial\alpha_{eq}^2$  is composed of quasi-linear diffusion rates that depend on the wave intensity and dispersion [see examples in *Glauert and Horne*, 2005; *Albert*, 2008; *Shprits and Ni*, 2009]. Therefore, Eq.(11) can be readily incorporated



into existing numerical codes solving diffusion equations. The resultant combined equation would include three operators  $\partial\Psi/\partial t = T_D\hat{D}\Psi + T_L\hat{L}\Psi + T_K\hat{K}\Psi$  where coefficients  $T_D$ ,  $T_L$ , and  $T_K$  define the relative time intervals of spacecraft observations of low-intensity ( $\mathcal{B}_w < 2$ , quasi-linear regime), high-intensity long wave-packets ( $\mathcal{B}_w > 2$ ,  $\beta^* > 50$ , nonlinear regime), and high-intensity short wave-packets ( $\mathcal{B}_w > 2$ ,  $\beta^* < 50$ , nonlinear regime) waves. The operator  $\hat{K}$  describing the combined action of nonlinear trapping and scattering by short wave-packets has been derived by *Mourenas et al.* [2018] and amounts to a simple drift term  $\hat{K} = -W_\gamma\partial\Psi/\partial\gamma - W_\alpha\partial\Psi/\partial\alpha_{eq}$ . For existing Fokker-Planck numerical codes of the radiation belt dynamics, the operator  $\hat{L}$  can be considered as a source/loss operator [similar to the  $\tau$ -operator describing particle losses  $\partial\Psi/\partial t \sim -\Psi/\tau$  - e.g., see *Horne et al.*, 2005; *Balikhin et al.*, 2012; *Mourenas et al.*, 2014].

### 6.3. Energy conservation

The evolution of the electron distribution function due to the nonlinear wave-particle interaction includes a rapid change of the total electron energy (see Fig. 9(left panel)). However, the energy of a whistler-mode wave is usually not sufficiently large to provide such a deceleration/acceleration [see discussion and estimates in *Shklyar*, 2011] and thus scattered (decelerated) electrons are the only available energy source for trapped electron acceleration. This balance imposes certain constraints on the initial electron distribution function for models describing nonlinear resonances. This initial distribution should be consistent with conservation of the total energy for solutions of Eq. (11). Figure 9(left panel) shows that one cannot easily reduce the rate of the total energy decrease simply by choosing a different electron energy distribution. We further checked the total particle energy variation for different initial pitch-angle distributions. Figure 9(right panel) shows

that an initial distribution with transverse anisotropy ( $\Psi \sim \sin \alpha_{eq}$ ) immediately loses energy, whereas a field-aligned anisotropic distribution ( $\Psi \sim \cos \alpha_{eq}$ ) first gains energy before losing it. We also checked more specific distributions (butterfly  $\Psi \sim \sin 2\alpha_{eq}$  sometime observed in the radiation belts [see statistics in *Ásnes et al.*, 2005] and a distribution with field-aligned beams  $\Psi \sim \sin \alpha_{eq} \cos^4 \alpha_{eq}$  observed during particle injections [e.g., *Mozer et al.*, 2016]). Both show energy increase during the first stage of the evolution. This suggests that for a  $\Psi$  to result in total energy conservation it should be more isotropic (i.e., something between transversely anisotropic  $\sim \sin \alpha_{eq}$  and field-aligned anisotropy  $\sim \cos \alpha_{eq}$ ). Moreover, under realistic conditions, particle anisotropy is energy dependent, and can be different for  $< 100$  keV particles and  $\sim 1$  MeV particles. Therefore, further investigations of particle distributions supporting the assumption of total energy conservation are needed for an accurate modelling the nonlinear wave-particle interaction [see, also, *Shklyar*, 2017, for details on the relation between trapped and scattered electron populations in a system with small variation of wave intensity].

## 7. Conclusions

We investigated the nonlinear resonant electron interaction with intense whistler-mode waves in the outer radiation belt. Combining THEMIS and Van Allen Probe observations of long and intense chorus wave-packets with the analytical theory of the resonant wave-particle interaction, we constructed a generalized kinetic equation that describes the evolution of the electron distribution function. The main conclusions of this study are:

- The observed occurrence rate and characteristics (amplitude, frequency) of intense parallel chorus waves may provide a very rapid (over tens of minutes) electron acceleration in the outer radiation belt. But such a rapid acceleration should be observed only

sporadically and locally, during time intervals of plasma injection and strong wave generation. Otherwise, the combination of very small time-averaged occurrence rate of long and intense chorus wave-packets and various other effects moderating their efficacy, lead to acceleration, occurring over typical times scales  $> 3 - 4$  hours similar to, or possibly larger than, quasi-linear diffusion time scales.

- Nonlinear trapping and scattering cause an extremely intense energy exchange between different particle populations. In the absence of a fine balance between these different particle populations, particle acceleration (deceleration) would immediately result in intense wave damping (growth). Thus, the observations of intense chorus wave emissions during many periods of resonant interaction suggest that these waves may be accompanied by particular (balanced) distribution of electrons, evolving with almost no variation of their total energy.

- Nonlinear effects of the wave-particle interaction can be included into modern codes of radiation belt dynamics, but to exclude unrealistically large particle acceleration/deceleration, such effects should be considered only with properly chosen initial particle distributions.

## Appendix A: probability of trapping

In this Appendix we derive the probability of electron trapping into resonance [see details in, e.g., *Artemyev et al.*, 2015c, 2018]. We start with Hamiltonian (2) and follow the proposed in *Neishtadt* [1999]. First, we introduce the momentum  $I$  conjugate to phase  $\zeta = \phi + \psi$ . We use generating function  $S_1 = P_z z + I(\phi + \psi) + \tilde{I}_x \psi$  where  $P_z = p_z - kI$  and  $\tilde{I}_x = I_x - I$  are new momenta conjugate to unchanged coordinates  $z$  and  $\psi$ . The new

Hamiltonian  $F = H + \partial S_1/\partial t$  is

$$F = -\omega I + m_e c^2 \gamma + U_w(z, \tilde{I}_x + I) \sin \zeta$$

$$\gamma = \sqrt{1 + \frac{(P_z + kI)^2}{m_e^2 c^2} + \frac{2\Omega_{ce}}{m_e c^2} (\tilde{I}_x + I)} \quad (12)$$

Hamiltonian (12) does not depend on  $\psi$ , and thus  $\tilde{I}_x$  is constant (we chose  $\tilde{I}_x = 0$ , i.e.,  $I = I_x$  at the initial time). Moreover, Hamiltonian (12) does not explicitly depend on time either ( $\zeta$  is a new variable), and thus  $F = \text{const}$ . This constant can be written as  $F/m_e c^2 = \varepsilon_0 = \gamma - \omega(\gamma^2 - 1) \sin^2 \alpha_{eq}/2\Omega_{ce}(0)$ , where we took into account that  $I_x = (1/2)(\gamma^2 - 1) \sin^2 \alpha_{eq}/\Omega_{ce}(0)$  and  $I = I_x$ . The resonance condition ( $\dot{\zeta} = 0$ ) for Hamiltonian (12) is

$$\frac{\partial F}{\partial I} = -\omega + \frac{k(P_z + kI)}{m_e \gamma} + \frac{\Omega_{ce}}{\gamma} = 0 \quad (13)$$

Combination of Eq. (12) and Eq. (13) gives for  $I = I_R(z, P_z)$  at the resonance:

$$\frac{\omega I_R}{m_e c^2} = -\frac{\varpi}{N^2} - \frac{P_z}{N m_e c} + \frac{1}{N \sqrt{N^2 - 1}} \sqrt{1 - \frac{\varpi^2}{N^2} - 2 \frac{\varpi}{N} \frac{P_z}{m_e c}} \quad (14)$$

where  $N = k(z)c/\omega$ ,  $\varpi = \Omega_{ce}(z)/\omega$ . Substituting Eq. (14) into  $\gamma$  from Eq. (12), we obtain the resonant energy:

$$\gamma_R = \frac{N}{\sqrt{N^2 - 1}} \sqrt{1 - \frac{\varpi^2}{N^2} - 2 \frac{\varpi}{N} \frac{P_z}{m_e c}} \quad (15)$$

Taking into account that  $\varepsilon_0 = -\omega I_R/m_e c^2 + \gamma_R = \text{const}$ , we exclude  $P_z$  from the equation for energy  $\gamma_R$ :

$$\gamma_R = \left| \varpi \mp \frac{N}{\sqrt{N^2 - 1}} \sqrt{1 - 2\varepsilon_0 \varpi + \varpi^2} \right| \quad (16)$$

Then, we expand Hamiltonian (12) around the resonant momentum:

$$F = \Lambda + \frac{1}{2} g (I - I_R)^2 + U_w(z, I_R) \sin \zeta, \quad (17)$$

$$\Lambda = -\omega I_R + m_e c^2 \gamma_R, \quad g = \left. \frac{\partial^2 \gamma}{\partial I^2} \right|_{I_R} = \frac{\omega^2 (N^2 - 1)}{\gamma_R^3 m_e c^2}$$

Hamiltonian  $\Lambda(z, P_z)$  describes resonant particle motion in the  $(z, P_z)$  plane. We use generating function  $S_2 = (I - I_R)\zeta + pz$  to introduce new momenta  $P_\zeta = I - I_R$ ,  $p = P_z - (\partial I_R / \partial z)\zeta$ , and new coordinate  $s = z + (\partial I_R / \partial P_z)\zeta$ . Near the resonance  $|(\partial I_R / \partial z)\zeta| \ll 1$ ,  $|(\partial I_R / \partial P_z)\zeta| \ll 1$  and we can expand the new Hamiltonian as [see details in, e.g., *Neishtadt, 1999; Neishtadt et al., 2011*]

$$\begin{aligned}\tilde{F} &= \Lambda(P_z, z) + \frac{1}{2}gP_\zeta^2 + U_{w,R} \sin \zeta = \Lambda(p, s) + H_\zeta \\ H_\zeta &= \frac{1}{2}gP_\zeta^2 - r\zeta + U_{w,R} \sin \zeta \\ U_{w,R} &= \frac{\sqrt{2(\gamma_R - \varepsilon_0)\varpi}}{\gamma_R N} \frac{eB_w}{m_e c \omega}\end{aligned}\tag{18}$$

Here  $r = \{\Lambda, I_R\}_{z, P_z}$  is the Poisson brackets for  $\Lambda$ ,  $I_R$ . Hamiltonian  $H_\zeta$  describes particle motion in the resonant phase plane  $(P_\zeta, \zeta)$  with coefficients depending on  $(p, s)$  as on parameters. Dynamics of  $(p, s)$  is described by Hamiltonian  $\Lambda(s, p)$ . The coefficient  $r$  is [see details in, e.g., *Artemyev et al., 2018*]

$$\begin{aligned}r &= \left( \frac{\partial \Lambda}{\partial z} \frac{\partial I_R}{\partial P_z} - \frac{\partial \Lambda}{\partial P_z} \frac{\partial I_R}{\partial z} \right)_{\substack{P_z \approx p \\ z \approx s}} = m_e c^2 \left( \frac{\partial \gamma_R}{\partial z} \frac{\partial I_R}{\partial P_z} - \frac{\partial \gamma_R}{\partial P_z} \frac{\partial I_R}{\partial z} \right) \\ &= \frac{m_e c^2}{2\gamma_R} \frac{N^2 D}{N^2 - 1} \left( 1 - \gamma_R^2 + \frac{\gamma_R^2 - \varpi^2}{N^2} + 2 \frac{(\gamma_R - \varpi)^2}{N^2} \frac{\partial \ln N}{\partial \ln \varpi} \right)\end{aligned}\tag{19}$$

Here  $D = (c/\omega N) \partial \ln \Omega_{ce} / \partial s$  is the ratio of the spatial scales. To define the probability of trapping, we introduce the area in the  $(P_\zeta, \zeta)$  plane filled by trapped particle trajectories,  $S_{res} = \oint P_\zeta d\zeta$ :

$$S_{res} = \sqrt{\frac{8r}{g}} \int_{\zeta_-}^{\zeta_+} \sqrt{a(\sin \zeta_+ - \sin \zeta) - (\zeta_+ - \zeta)} d\zeta\tag{20}$$

where  $a = |U_{w,R}/r|$ , and integration limits,  $\zeta_\pm = \zeta_\pm(s)$ , are solutions of equations  $a \cos \zeta_+ = 1$  and  $a(\sin \zeta_+ - \sin \zeta_-) - (\zeta_+ - \zeta_-) = 0$ . For  $|D| \ll 1$ , the probability of

trapping is [see *Neishtadt*, 1975, 1999]:

$$\Pi = \frac{1}{2\pi|r|} \left( \frac{\partial\Lambda}{\partial s} \frac{\partial S_{res}}{\partial p} - \frac{\partial\Lambda}{\partial p} \frac{\partial S_{res}}{\partial s} \right) = \frac{\{\Lambda, S_{res}\}_{s,p}}{2\pi|r|} \quad (21)$$

This probability is small:  $\Pi \sim \sqrt{|D|}$ . Numerical verifications of Eq. (21) can be found in Fig. 4 and *Artemyev et al.* [2013, 2015c].

## Appendix B: trapped particle acceleration

In this Appendix we estimate the acceleration rate of trapped particles. We would like to determine the energy change  $\Delta\gamma_{trap}$  due to trapping as a function of the initial particle energy and pitch-angle,  $(\gamma, \alpha_{eq})$  (the corresponding pitch-angle change is defined by Eq. (6)). To be trapped, a particle should resonate with the wave at a location where the probability of trapping  $\Pi > 0$ . Equation (21) shows that  $\Pi$  is proportional to the change of  $S_{res}$  along the resonant trajectory:  $dS_{res}/dt = \partial S_{res}/\partial t + \{\Lambda, S_{res}\}_{s,p}$ . Therefore, particles become trapped at some  $S_{res,trap}$  with  $dS_{res,trap}/dt > 0$ .

Dynamics of trapped particles are defined by the Hamiltonian  $H_\zeta$  in Eq. (18). This is a classical pendulum Hamiltonian with coefficients depending on slowly changing parameters  $(s, p)$  determined by Hamiltonian  $\Lambda$  in Eq. (18) (note that the time scale of  $(s, p)$  variation is much larger than the time scale of  $(\zeta, P_\zeta)$  variations [see details in, e.g., *Neishtadt*, 1999; *Artemyev et al.*, 2015c]). The phase portrait of Hamiltonian  $H_\zeta$  is shown in Fig. 10(a). There are closed trajectories oscillating around the resonance  $P_\zeta = 0$  (trapped trajectories) confined by the separatrix  $\mathcal{S}$ . The area surrounded by the separatrix,  $S_{res}$ , changes with time (with  $(s, p)$ ) and when this area becomes larger than the area surrounded by the particle trajectory,  $2\pi I_\zeta$ , particles become trapped (this determines the condition of  $dS_{res}/dt > 0$ ). The area  $2\pi I_\zeta = \oint P_\zeta d\zeta$  (integrated along a

particle trajectory) is the adiabatic invariant of the system described by Hamiltonian  $H_\zeta$  [e.g., *Landau and Lifshitz*, 1988] and thus,  $I_\zeta$  is conserved during trapped motion. The equation  $I_\zeta = \text{const}$  defines the condition for particle escape from resonance:  $2\pi I_\zeta = S_{res}$  and  $dS_{res}/dt < 0$ . Thus, the position of particle escape from the resonance,  $z_{esc}$ , is determined by equation  $S_{res,trap} = S_{res,esc}$  and  $dS_{res,esc}/dt < 0$  (see scheme in Fig. 10(b)). The energy gain of trapped particles is  $\Delta\gamma_{trap} = \gamma_R(z_{esc}) - \gamma_R(z_{trap})$  with  $\gamma_R$  given by Eq. (16). To construct  $\Delta\gamma_{trap}(\gamma, \alpha_{eq})$ , we determine the  $S_{res}$  profile along the resonant trajectory (Eq. (20)) for each  $(\gamma, \alpha_{eq})$ , define positions of particle trapping and escape, and calculate the difference of the resonant energy  $\gamma_R$  between these positions.

Figure 10(c,d) compares analytical predictions of trapped particle motion with results of the numerical integration of Hamiltonian equations. Panel (c) demonstrates that trapped particle energy (black curve) coincides with Eq. (16) (red curve). Particle becomes trapped and escape from the resonance with the same area  $S_{res}$  (grey curve). During the trapped motion, the particle oscillates in the  $(\zeta, P_\zeta)$  plane (panel (d)) and the area surrounded by the particle trajectory is conserved (blue crosses in panel (c)). This area,  $2\pi I_\zeta$ , is equal to  $S_{res,trap}$  and thus equation  $2\pi I_\zeta = S_{res}$  defines the position of particle escape from resonance.

### Appendix C: scattering amplitude

In this Appendix we estimate the particle energy change due to nonlinear scattering,  $\Delta\gamma_{scat}$ . The conservation of  $\varepsilon_0 = \gamma - \omega I/m_e c^2$  shows that  $\Delta\gamma = \omega\Delta I/m_e c^2$ . To evaluate  $\Delta I$ , we consider Hamiltonian (12):

$$\Delta I = -2 \int_{-\infty}^{t_R} \frac{\partial F}{\partial \zeta} dt = -2 \int_{-\infty}^{\zeta_+} U_{w,R} \cos \zeta \frac{d\zeta}{gP_\zeta} \quad (22)$$

$$= -\sqrt{\frac{2U_{w,R}}{g}} \int_{-\infty}^{\zeta_+} \frac{\sqrt{a} \cos \zeta}{\sqrt{a(\sin \zeta_+ - \sin \zeta) - (\zeta_+ - \zeta)}} d\zeta$$

where  $t_R$  is the time of the resonant interaction and we use  $dt = d\zeta/\dot{\zeta} = d\zeta/gP_\zeta$  (see Hamiltonian  $H_\zeta$  in Eq. (18)). The change  $\Delta I$  depends on the phase  $\zeta_+$ , or alternatively on  $\xi$ , where  $2\pi\xi = a \sin \zeta_+ - \zeta_+$ . It can be shown that  $\Delta I$  is a periodic function of  $\xi$  [see, e.g., *Karpman et al.*, 1975; *Neishtadt*, 1999; *Artemyev et al.*, 2014b] and  $\xi$  is distributed uniformly for any reasonable initial set of wave phases  $\zeta$  [e.g., *Itin et al.*, 2000]. Therefore, to derive the average value of the energy change  $\Delta\gamma_{scat} = \omega\langle\Delta I\rangle_\xi/m_e c^2$  we need to average  $\Delta I$  over  $\xi \in [0, 1]$ . An important property of the function  $\Delta I(\xi)$  is  $\langle\Delta I\rangle_\xi = -S_{res}/2\pi$  [see *Karpman et al.*, 1975; *Neishtadt*, 1999; *Dolgopyat*, 2012]. Thus, we can express  $\Delta\gamma_{scat}$  as:

$$\Delta\gamma_{scat} = \frac{\omega}{m_e c^2} \langle\Delta I\rangle_\xi = -\frac{\omega}{m_e c^2} \frac{S_{res}}{2\pi} \quad (23)$$

Equation (23) shows that  $\Delta\gamma_{scat}$  is about  $\sqrt{|D|} \ll 1$ , i.e.,  $\Delta\gamma_{scat}$  is of the same order as the probability of trapping  $\Pi \sim \sqrt{|D|}$  [see a discussion in *Shklyar and Matsumoto*, 2009; *Shklyar*, 2011].

**Acknowledgments.** This material is based in part upon work supported by the National Science Foundation under Award No. CMMI-1740777 (D.L.V.). X.J.Z., A.V.A., and V.A. acknowledge NASA contract NAS5-02099 for use of data from the THEMIS Mission, specifically J. W. Bonnell and F. S. Mozer for use of EFI data, A. Roux and O. LeContel for use of SCM data, and K. H. Glassmeier, U. Auster and W. Baumjohann for the use of FGM data provided under the lead of the Technical University of Braunschweig and with financial support through the German Ministry for Economy and Technology and the German Center for Aviation and Space (DLR) under contract 50 OC 0302. The work of X.J.Z. was also supported by RBSP-EMFISIS



and RBSP-ECT funding 443956-TH-81074 and 443956-TH-79425 under NASA's prime contract No. NNN06AA01C. We acknowledge the Van Allen Probes EMFISIS data obtained from <https://emfisis.physics.uiowa.edu/data/index>, and THEMIS data from <http://themis.ssl.berkeley.edu/>. We also thank the World Data Center for Geomagnetism, Kyoto for providing AE index, and the Space Physics Data Facility at the NASA Goddard Space Flight Center for providing the OMNI data used in this study.

## References

- Åsnes, A., R. W. Friedel, J. Stadsnes, M. Thomsen, N. Østgaard, and T. Cayton, Statistical pitch angle properties of substorm-injected electron clouds and their relation to dawnside energetic electron precipitation, *J. Geophys. Res.*, , *110*, A05207, doi:10.1029/2004JA010838, 2005.
- Agapitov, O., A. Artemyev, V. Krasnoselskikh, Y. V. Khotyaintsev, D. Mourenas, H. Breuillard, M. Balikhin, and G. Rolland, Statistics of whistler mode waves in the outer radiation belt: Cluster STAFF-SA measurements, *J. Geophys. Res.*, , *118*, 3407–3420, doi:10.1002/jgra.50312, 2013.
- Agapitov, O., A. Artemyev, D. Mourenas, V. Krasnoselskikh, J. Bonnell, O. Le Contel, C. M. Cully, and V. Angelopoulos, The quasi-electrostatic mode of chorus waves and electron nonlinear acceleration, *J. Geophys. Res.*, , *119*, 16061626, doi:10.1002/2013JA019223, 2014a.
- Agapitov, O., L. W. Blum, F. S. Mozer, J. W. Bonnell, and J. Wygant, Chorus whistler wave source scales as determined from multipoint Van Allen Probe measurements, *Geophys. Res. Lett.*, , *44*, 2634–2642, doi:10.1002/2017GL072701, 2017.

Agapitov, O. V., A. V. Artemyev, D. Mourenas, Y. Kasahara, and V. Krasnoselskikh, Inner belt and slot region electron lifetimes and energization rates based on AKEBONO statistics of whistler waves, *J. Geophys. Res.*, , 119, 2876–2893, doi:10.1002/2014JA019886, 2014b.

Agapitov, O. V., A. V. Artemyev, D. Mourenas, F. S. Mozer, and V. Krasnoselskikh, Nonlinear local parallel acceleration of electrons through Landau trapping by oblique whistler mode waves in the outer radiation belt, *Geophys. Res. Lett.*, , 42, 10, doi:10.1002/2015GL066887, 2015a.

Agapitov, O. V., A. V. Artemyev, D. Mourenas, F. S. Mozer, and V. Krasnoselskikh, Empirical model of lower band chorus wave distribution in the outer radiation belt, *J. Geophys. Res.*, , 120, 10, doi:10.1002/2015JA021829, 2015b.

Agapitov, O. V., D. Mourenas, A. V. Artemyev, and F. S. Mozer, Exclusion principle for very oblique and parallel lower band chorus waves, *Geophys. Res. Lett.*, , 43(21), 11,112–11,120, doi:10.1002/2016GL071250, 2016.

Albert, J. M., Cyclotron resonance in an inhomogeneous magnetic field, *Physics of Fluids B*, 5, 2744–2750, doi:10.1063/1.860715, 1993.

Albert, J. M., Nonlinear interaction of outer zone electrons with VLF waves, *Geophys. Res. Lett.*, , 29, 1275, doi:10.1029/2001GL013941, 2002.

Albert, J. M., Efficient approximations of quasi-linear diffusion coefficients in the radiation belts, *J. Geophys. Res.*, , 113, A06208, doi:10.1029/2007JA012936, 2008.

Albert, J. M., Diffusion by one wave and by many waves, *J. Geophys. Res.*, , 115, A00F05, doi:10.1029/2009JA014732, 2010.

Albert, J. M., M. J. Starks, R. B. Horne, N. P. Meredith, and S. A. Glauert, Quasi-linear simulations of inner radiation belt electron pitch angle and energy distributions, *Geophys. Res. Lett.*, , *43*, 2381–2388, doi:10.1002/2016GL067938, 2016.

Andronov, A. A., and V. Y. Trakhtengerts, Kinetic instability of the Earth's outer radiation belt, *Geomagnetism and Aeronomy*, *4*, 233–242, 1964.

Angelopoulos, V., The THEMIS Mission, *Space Sci. Rev.*, *141*, 5–34, doi:10.1007/s11214-008-9336-1, 2008.

Artemyev, A., V. Krasnoselskikh, O. Agapitov, D. Mourenas, and G. Rolland, Non-diffusive resonant acceleration of electrons in the radiation belts., *Physics of Plasmas*, *19*, 122,901, doi:10.1063/1.4769726, 2012.

Artemyev, A., O. Agapitov, D. Mourenas, V. Krasnoselskikh, V. Shastun, and F. Mozer, Oblique whistler-mode waves in the earth's inner magnetosphere: Energy distribution, origins, and role in radiation belt dynamics, *Space Science Reviews*, *200*, 261–355, doi:10.1007/s11214-016-0252-5, 2016.

Artemyev, A. V., A. A. Vasiliev, D. Mourenas, O. Agapitov, and V. Krasnoselskikh, Non-linear electron acceleration by oblique whistler waves: Landau resonance vs. cyclotron resonance., *Physics of Plasmas*, *20*, 122,901, doi:10.1063/1.4836595, 2013.

Artemyev, A. V., A. A. Vasiliev, D. Mourenas, O. Agapitov, V. Krasnoselskikh, D. Boscher, and G. Rolland, Fast transport of resonant electrons in phase space due to nonlinear trapping by whistler waves, *Geophys. Res. Lett.*, , *41*, 57275733, doi:10.1002/2014GL061380, 2014a.

Artemyev, A. V., A. A. Vasiliev, D. Mourenas, O. V. Agapitov, and V. V. Krasnoselskikh, Electron scattering and nonlinear trapping by oblique whistler waves: The

critical wave intensity for nonlinear effects, *Physics of Plasmas*, *21*(10), 102903, doi:10.1063/1.4897945, 2014b.

Artemyev, A. V., O. V. Agapitov, D. Mourenas, V. V. Krasnoselskikh, and F. S. Mozer, Wave energy budget analysis in the Earth's radiation belts uncovers a missing energy, *Nature Communications*, *6*, 8143, doi:10.1038/ncomms8143, 2015a.

Artemyev, A. V., D. Mourenas, O. V. Agapitov, D. L. Vainchtein, F. S. Mozer, and V. V. Krasnoselskikh, Stability of relativistic electron trapping by strong whistler or electromagnetic ion cyclotron waves, *Physics of Plasmas*, *22*, 082901, doi:10.1063/1.4927774, 2015b.

Artemyev, A. V., A. A. Vasiliev, D. Mourenas, A. I. Neishtadt, O. V. Agapitov, and V. Krasnoselskikh, Probability of relativistic electron trapping by parallel and oblique whistler-mode waves in Earth's radiation belts, *Physics of Plasmas*, *22*(11), 112903, doi:10.1063/1.4935842, 2015c.

Artemyev, A. V., A. I. Neishtadt, A. A. Vasiliev, and D. Mourenas, Kinetic equation for nonlinear resonant wave-particle interaction, *Physics of Plasmas*, *23*(9), 090701, doi:10.1063/1.4962526, 2016.

Artemyev, A. V., A. I. Neishtadt, A. A. Vasiliev, and D. Mourenas, Long-term evolution of electron distribution function due to nonlinear resonant interaction with whistler mode waves, *Journal of Plasma Physics*, p. submitted, 2018.

Auster, H. U., et al., The THEMIS Fluxgate Magnetometer, *Space Sci. Rev.*, *141*, 235–264, doi:10.1007/s11214-008-9365-9, 2008.

Balikhin, M. A., M. Gedalin, G. D. Reeves, R. J. Boynton, and S. A. Billings, Time scaling of the electron flux increase at GEO: The local energy diffusion model vs observations,

*J. Geophys. Res.*, , 117, A10208, doi:10.1029/2012JA018114, 2012.

Bell, T. F., The nonlinear gyroresonance interaction between energetic electrons and coherent VLF waves propagating at an arbitrary angle with respect to the earth's magnetic field, *J. Geophys. Res.*, , 89, 905–918, doi:10.1029/JA089iA02p00905, 1984.

Bell, T. F., The wave magnetic field amplitude threshold for nonlinear trapping of energetic gyroresonant and Landau resonant electrons by nonducted VLF waves in the magnetosphere, *J. Geophys. Res.*, , 91, 4365–4379, doi:10.1029/JA091iA04p04365, 1986.

Bonnell, J. W., F. S. Mozer, G. T. Delory, A. J. Hull, R. E. Ergun, C. M. Cully, V. Angelopoulos, and P. R. Harvey, The Electric Field Instrument (EFI) for THEMIS, *Space Sci. Rev.*, 141, 303–341, doi:10.1007/s11214-008-9469-2, 2008.

Bortnik, J., R. M. Thorne, and U. S. Inan, Nonlinear interaction of energetic electrons with large amplitude chorus, *Geophys. Res. Lett.*, , 35, L21102, doi:10.1029/2008GL035500, 2008.

Demekhov, A. G., Generation of VLF emissions with the increasing and decreasing frequency in the magnetosperic cyclotron maser in the backward wave oscillator regime, *Radiophysics and Quantum Electronics*, 53, 609–622, doi:10.1007/s11141-011-9256-x, 2011.

Demekhov, A. G., V. Y. Trakhtengerts, M. Rycroft, and D. Nunn, Efficiency of electron acceleration in the Earth's magnetosphere by whistler mode waves, *Geomagnetism and Aeronomy*, 49, 24–29, doi:10.1134/S0016793209010034, 2009.

Demekhov, A. G., U. Taubenschuss, and O. Santolík, Simulation of VLF chorus emissions in the magnetosphere and comparison with THEMIS spacecraft data, *J. Geophys. Res.*, , 122, 166–184, doi:10.1002/2016JA023057, 2017.

Dolgopyat, D., Repulsion from Resonances, in *Memoires De La Societe Mathematique De France, Memoires De La Societe Mathematique De France*, vol. 128, 2012.

Drozdo, A. Y., Y. Y. Shprits, K. G. Orlova, A. C. Kellerman, D. A. Subbotin, D. N. Baker, H. E. Spence, and G. D. Reeves, Energetic, relativistic, and ultrarelativistic electrons: Comparison of long-term VERB code simulations with Van Allen Probes measurements, *J. Geophys. Res.*, , 120, 3574–3587, doi:10.1002/2014JA020637, 2015.

Foster, J. C., P. J. Erickson, Y. Omura, D. N. Baker, C. A. Kletzing, and S. G. Claude-pierre, Van allen probes observations of prompt mev radiation belt electron acceleration in nonlinear interactions with vlf chorus, *Journal of Geophysical Research: Space Physics*, 122(1), 324–339, doi:10.1002/2016JA023429, 2017.

Glauert, S. A., and R. B. Horne, Calculation of pitch angle and energy diffusion coefficients with the PADIE code, *J. Geophys. Res.*, 110, A04206, doi:10.1029/2004JA010851, 2005.

Glauert, S. A., R. B. Horne, and N. P. Meredith, Three-dimensional electron radiation belt simulations using the BAS Radiation Belt Model with new diffusion models for chorus, plasmaspheric hiss, and lightning-generated whistlers, *J. Geophys. Res.*, , 119, 268–289, doi:10.1002/2013JA019281, 2014.

Horne, R. B., R. M. Thorne, S. A. Glauert, J. M. Albert, N. P. Meredith, and R. R. Anderson, Timescale for radiation belt electron acceleration by whistler mode chorus waves, *J. Geophys. Res.*, , 110, A03225, doi:10.1029/2004JA010811, 2005.

Hsieh, Y.-K., and Y. Omura, Nonlinear dynamics of electrons interacting with oblique whistler mode chorus in the magnetosphere, *J. Geophys. Res.*, , 122, 675–694, doi:10.1002/2016JA023255, 2017.

Hsieh, Y.-K., and Y. Omura, Study of wave-particle interactions for whistler mode waves at oblique angles by utilizing the gyroaveraging method, *Radio Science*, *52*(10), 1268–1281, doi:10.1002/2017RS006245, 2017RS006245, 2017.

Itin, A. P., A. I. Neishtadt, and A. A. Vasiliev, Captures into resonance and scattering on resonance in dynamics of a charged relativistic particle in magnetic field and electrostatic wave, *Physica D: Nonlinear Phenomena*, *141*, 281–296, doi:10.1016/S0167-2789(00)00039-7, 2000.

Karpman, V. I., Nonlinear Effects in the ELF Waves Propagating along the Magnetic Field in the Magnetosphere, *Space Sci. Rev.*, *16*, 361–388, doi:10.1007/BF00171564, 1974.

Karpman, V. I., and D. R. Shklyar, Particle precipitation caused by a single whistler-mode wave injected into the magnetosphere, *Plan. Space Sci.*, *25*, 395–403, doi:10.1016/0032-0633(77)90055-1, 1977.

Karpman, V. I., J. N. Istomin, and D. R. Shklyar, Nonlinear theory of a quasi-monochromatic whistler mode packet in inhomogeneous plasma, *Plasma Physics*, *16*, 685–703, doi:10.1088/0032-1028/16/8/001, 1974.

Karpman, V. I., I. N. Istomin, and D. R. Shklyar, Effects of nonlinear interaction of monochromatic waves with resonant particles in the inhomogeneous plasma, *Physica Scripta*, *11*, 278–284, doi:10.1088/0031-8949/11/5/008, 1975.

Kasahara, S., et al., Pulsating aurora from electron scattering by chorus waves, *Nature*, *554*, 337340, doi:10.1038/nature25505, 2018.

Katoh, Y., and Y. Omura, Computer simulation of chorus wave generation in the Earth's inner magnetosphere, *Geophys. Res. Lett.*, *34*, L03102, doi:10.1029/2006GL028594,

2007.

Kennel, C. F., and F. Engelmann, Velocity Space Diffusion from Weak Plasma Turbulence in a Magnetic Field, *Physics of Fluids*, *9*, 2377–2388, doi:10.1063/1.1761629, 1966.

Kennel, C. F., and H. E. Petschek, Limit on Stably Trapped Particle Fluxes, *J. Geophys. Res.*, , *71*, 1–28, 1966.

Kletzing, C. A., et al., The Electric and Magnetic Field Instrument Suite and Integrated Science (EMFISIS) on RBSP, *Space Sci. Rev.*, *179*, 127–181, doi:10.1007/s11214-013-9993-6, 2013.

Landau, L. D., and E. M. Lifshitz, *Vol. 1: Mechanics*, Course of Theoretical Physics, Oxford: Pergamon, 1988.

Le Contel, O., et al., First Results of the THEMIS Search Coil Magnetometers, *Space Sci. Rev.*, *141*, 509–534, doi:10.1007/s11214-008-9371-y, 2008.

Le Queau, D., and A. Roux, Quasi-monochromatic wave-particle interactions in magnetospheric plasmas, *Solar Phys.*, *111*, 59–80, doi:10.1007/BF00145441, 1987.

Li, W., et al., Characteristics of the Poynting flux and wave normal vectors of whistler-mode waves observed on THEMIS, *J. Geophys. Res.*, , *118*, 1461–1471, doi:10.1002/jgra.50176, 2013.

Li, W., et al., Radiation belt electron acceleration by chorus waves during the 17 March 2013 storm, *J. Geophys. Res.*, , *119*, 4681–4693, doi:10.1002/2014JA019945, 2014.

Li, W., et al., Radiation belt electron acceleration during the 17 March 2015 geomagnetic storm: Observations and simulations, *J. Geophys. Res.*, , *121*, 5520–5536, doi:10.1002/2016JA022400, 2016.

Lyons, L. R., and D. J. Williams, *Quantitative aspects of magnetospheric physics.*, 1984.



- Ma, Q., D. Mourenas, W. Li, A. Artemyev, and R. M. Thorne, VLF waves from ground-based transmitters observed by the Van Allen Probes: Statistical model and effects on plasmaspheric electrons, *Geophys. Res. Lett.*, , *44*, 6483–6491, doi:10.1002/2017GL073885, 2017a.
- Ma, Q., et al., Modeling inward diffusion and slow decay of energetic electrons in the Earth’s outer radiation belt, *Geophys. Res. Lett.*, , *42*, 987–995, doi:10.1002/2014GL062977, 2015.
- Ma, Q., et al., Characteristic energy range of electron scattering due to plasmaspheric hiss, *J. Geophys. Res.*, , *121*, 11, doi:10.1002/2016JA023311, 2016.
- Ma, Q., et al., Diffusive Transport of Several Hundred keV Electrons in the Earth’s Slot Region, *J. Geophys. Res.*, , *122*, 10, doi:10.1002/2017JA024452, 2017b.
- Mauk, B. H., N. J. Fox, S. G. Kanekal, R. L. Kessel, D. G. Sibeck, and A. Ukhorskiy, Science Objectives and Rationale for the Radiation Belt Storm Probes Mission, *Space Sci. Rev.*, *179*, 3–27, doi:10.1007/s11214-012-9908-y, 2013.
- Meredith, N. P., R. B. Horne, A. Sicard-Piet, D. Boscher, K. H. Yearby, W. Li, and R. M. Thorne, Global model of lower band and upper band chorus from multiple satellite observations, *J. Geophys. Res.*, , *117*, A10225, doi:10.1029/2012JA017978, 2012.
- Mourenas, D., A. V. Artemyev, O. V. Agapitov, and V. Krasnoselskikh, Consequences of geomagnetic activity on energization and loss of radiation belt electrons by oblique chorus waves, *J. Geophys. Res.*, , *119*, 2775–2796, doi:10.1002/2013JA019674, 2014.
- Mourenas, D., Q. Ma, A. V. Artemyev, and W. Li, Scaling laws for the inner structure of the radiation belts, *Geophys. Res. Lett.*, , *44*, 3009–3018, doi:10.1002/2017GL072987, 2017.

- Mourenas, D., X.-J. Zhang, A. V. Artemyev, V. Angelopoulos, R. M. Thorne, J. Bortnik, A. I. Neishtadt, and A. A. Vasiliev, Electron nonlinear resonant interaction with short and intense parallel chorus wave-packets, *J. Geophys. Res.*, , p. submitted, 2018.
- Mozer, F. S., A. Artemyev, O. V. Agapitov, D. Mourenas, and I. Vasko, Near-relativistic electron acceleration by Landau trapping in time domain structures, *Geophys. Res. Lett.*, , *43*, 508–514, doi:10.1002/2015GL067316, 2016.
- Neishtadt, A., Passage through a separatrix in a resonance problem with a slowly-varying parameter, *Journal of Applied Mathematics and Mechanics*, *39*, 594–605, doi:10.1016/0021-8928(75)90060-X, 1975.
- Neishtadt, A., A. Vasiliev, and A. Artemyev, Resonance-induced surfatron acceleration of a relativistic particle, *Moscow Mathematical Journal*, *11*(3), 531–545, 2011.
- Neishtadt, A. I., On Adiabatic Invariance in Two-Frequency Systems, in *Hamiltonian Systems with Three or More Degrees of Freedom*, ed. Sim C., NATO ASI Series C. Dordrecht: Kluwer Acad. Publ., *533*, 193–213, doi:10.1063/1.166236, 1999.
- Neishtadt, A. I., B. A. Petrovichev, and A. A. Chernikov, Particle entrainment into unlimited acceleration, *Soviet Journal of Plasma Physics*, *15*, 1021–1023, 1989.
- Ni, B., et al., Origins of the Earth’s Diffuse Auroral Precipitation, *Space Sci. Rev.*, doi:10.1007/s11214-016-0234-7, 2016.
- Nunn, D., Wave-particle interactions in electrostatic waves in an inhomogeneous medium, *Journal of Plasma Physics*, *6*, 291, doi:10.1017/S0022377800006061, 1971.
- Nunn, D., A self-consistent theory of triggered VLF emissions, *Plan. Space Sci.*, *22*, 349–378, doi:10.1016/0032-0633(74)90070-1, 1974.

- Nunn, D., A nonlinear theory of sideband stability in ducted whistler mode waves, *Plan. Space Sci.*, *34*, 429–451, doi:10.1016/0032-0633(86)90032-2, 1986.
- Nunn, D., and Y. Omura, A computational and theoretical investigation of nonlinear wave-particle interactions in oblique whistlers, *J. Geophys. Res.*, , *120*, 2890–2911, doi:10.1002/2014JA020898, 2015.
- O’Brien, T. P., and M. B. Moldwin, Empirical plasmopause models from magnetic indices, *Geophys. Res. Lett.*, , *30*, 1152, doi:10.1029/2002GL016007, 2003.
- Omura, Y., N. Furuya, and D. Summers, Relativistic turning acceleration of resonant electrons by coherent whistler mode waves in a dipole magnetic field, *J. Geophys. Res.*, , *112*, A06236, doi:10.1029/2006JA012243, 2007.
- Omura, Y., Y. Katoh, and D. Summers, Theory and simulation of the generation of whistler-mode chorus, *J. Geophys. Res.*, , *113*, A04223, doi:10.1029/2007JA012622, 2008.
- Omura, Y., D. Nunn, and D. Summers, Generation Processes of Whistler Mode Chorus Emissions: Current Status of Nonlinear Wave Growth Theory, in *Dynamics of the Earth’s Radiation Belts and Inner Magnetosphere*, edited by D. Summers, I. U. Mann, D. N. Baker, and M. Schulz, American Geophysical Union, pp. 243–254, doi:10.1029/2012GM001347, 2013.
- Omura, Y., Y. Miyashita, M. Yoshikawa, D. Summers, M. Hikishima, Y. Ebihara, and Y. Kubota, Formation process of relativistic electron flux through interaction with chorus emissions in the Earth’s inner magnetosphere, *J. Geophys. Res.*, , *120*, 9545–9562, doi:10.1002/2015JA021563, 2015.

Reeves, G. D., et al., Electron Acceleration in the Heart of the Van Allen Radiation Belts, *Science*, *341*, 6149, doi:10.1126/science.1237743, 2013.

Schulz, M., and L. J. Lanzerotti, *Particle diffusion in the radiation belts*, Springer, New York, 1974.

Shklyar, D., and H. Matsumoto, Oblique Whistler-Mode Waves in the Inhomogeneous Magnetospheric Plasma: Resonant Interactions with Energetic Charged Particles, *Surveys in Geophysics*, *30*, 55–104, doi:10.1007/s10712-009-9061-7, 2009.

Shklyar, D. R., Stochastic motion of relativistic particles in the field of a monochromatic wave, *Sov. Phys. JETP*, *53*, 1197–1192, 1981.

Shklyar, D. R., On the nature of particle energization via resonant wave-particle interaction in the inhomogeneous magnetospheric plasma, *Annales Geophysicae*, *29*, 1179–1188, doi:10.5194/angeo-29-1179-2011, 2011.

Shklyar, D. R., Energy transfer from lower energy to higher-energy electrons mediated by whistler waves in the radiation belts, *J. Geophys. Res.*, , *122*(1), 640–655, doi:10.1002/2016JA023263, 2017.

Shklyar, D. R., and G. Zimbardo, Particle dynamics in the field of two waves in a magnetoplasma, *Plasma Physics and Controlled Fusion*, *56*(9), 095002, doi:10.1088/0741-3335/56/9/095002, 2014.

Shprits, Y. Y., and B. Ni, Dependence of the quasi-linear scattering rates on the wave normal distribution of chorus waves, *J. Geophys. Res.*, , *114*, A11205, doi:10.1029/2009JA014223, 2009.

Solovov, V. V., and D. R. Shklyar, Particle heating by a low-amplitude wave in an inhomogeneous magnetoplasma, *Sov. Phys. JETP*, *63*, 272–277, 1986.

Su, Z., et al., Quantifying the relative contributions of substorm injections and chorus waves to the rapid outward extension of electron radiation belt, *J. Geophys. Res.*, , *119*(12), 10,023–10,040, doi:10.1002/2014JA020709, 2014JA020709, 2014.

Subbotin, D. A., Y. Y. Shprits, and B. Ni, Long-term radiation belt simulation with the VERB 3-D code: Comparison with CRRES observations, *J. Geophys. Res.*, , *116*, A12210, doi:10.1029/2011JA017019, 2011.

Summers, D., and Y. Omura, Ultra-relativistic acceleration of electrons in planetary magnetospheres, *Geophys. Res. Lett.*, , *34*, L24205, doi:10.1029/2007GL032226, 2007.

Summers, D., R. M. Thorne, and F. Xiao, Relativistic theory of wave-particle resonant diffusion with application to electron acceleration in the magnetosphere, *J. Geophys. Res.*, , *103*, 20,487–20,500, doi:10.1029/98JA01740, 1998.

Tao, X., R. M. Thorne, W. Li, B. Ni, N. P. Meredith, and R. B. Horne, Evolution of electron pitch angle distributions following injection from the plasma sheet, *J. Geophys. Res.*, , *116*, A04229, doi:10.1029/2010JA016245, 2011.

Tao, X., J. Bortnik, J. M. Albert, and R. M. Thorne, Comparison of bounce-averaged quasi-linear diffusion coefficients for parallel propagating whistler mode waves with test particle simulations, *J. Geophys. Res.*, , *117*, A10205, doi:10.1029/2012JA017931, 2012.

Tao, X., J. Bortnik, J. M. Albert, R. M. Thorne, and W. Li, The importance of amplitude modulation in nonlinear interactions between electrons and large amplitude whistler waves, *Journal of Atmospheric and Solar-Terrestrial Physics*, *99*, 67–72, doi:10.1016/j.jastp.2012.05.012, 2013.

Tao, X., F. Zonca, and L. Chen, Identify the nonlinear wave-particle interaction regime in rising tone chorus generation, *Geophys. Res. Lett.*, , *44*(8), 3441–3446, doi:10.1002/

2017GL072624, 2017.

Thorne, R. M., B. Ni, X. Tao, R. B. Horne, and N. P. Meredith, Scattering by chorus waves as the dominant cause of diffuse auroral precipitation, *Nature*, *467*, 943–946, doi:10.1038/nature09467, 2010.

Thorne, R. M., et al., Rapid local acceleration of relativistic radiation-belt electrons by magnetospheric chorus, *Nature*, *504*, 411–414, doi:10.1038/nature12889, 2013.

Tsurutani, B. T., B. J. Falkowski, O. P. Verkhoglyadova, J. S. Pickett, O. Santolík, and G. S. Lakhina, Quasi-coherent chorus properties: 1. Implications for wave-particle interactions, *J. Geophys. Res.*, , *116*, A09210, doi:10.1029/2010JA016237, 2011.

Van Kampen, N. G., *Stochastic Processes in Physics and Chemistry*, 3 ed., North Holland, 2003.

Vedenov, A. A., E. Velikhov, and R. Sagdeev, Quasilinear theory of plasma oscillations, *Nuclear Fusion Suppl.*, *2*, 465475, 1962.

Wygant, J. R., et al., The Electric Field and Waves Instruments on the Radiation Belt Storm Probes Mission, *Space Sci. Rev.*, *179*, 183–220, doi:10.1007/s11214-013-0013-7, 2013.

Yang, C., F. Xiao, Y. He, S. Liu, Q. Zhou, M. Guo, and W. Zhao, Storm-time evolution of outer radiation belt relativistic electrons by a nearly continuous distribution of chorus, *Geophys. Res. Lett.*, , pp. n/a–n/a, doi:10.1002/2017GL075894, 2017GL075894, 2018.

Yoon, P. H., V. S. Pandey, and D.-H. Lee, Relativistic electron acceleration by oblique whistler waves, *Physics of Plasmas*, *20*(11), 112902, doi:10.1063/1.4831965, 2013.

Zhang, X.-J., R. Thorne, A. Artemyev, D. Mourenas, V. Angelopoulos, and J. Bortnik, Properties of intense field-aligned whistler waves: implications for nonlinear wave-

particle interaction., *J. Geophys. Res.*, , p. submitted, 2018.

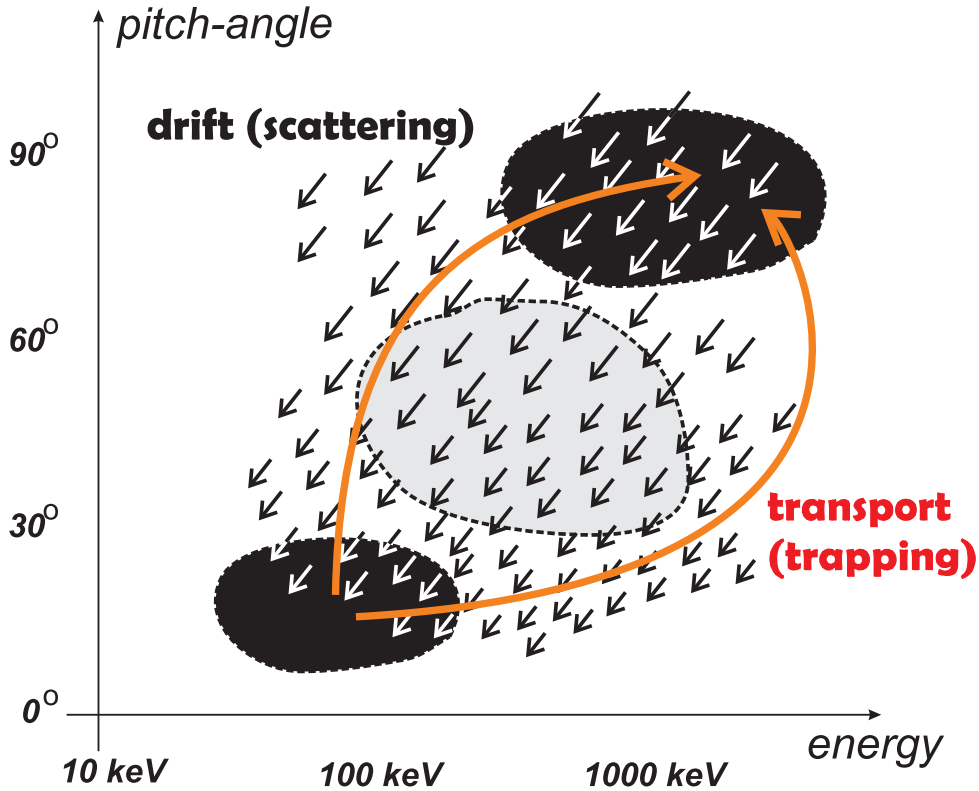


**Figure 1.** A schematic view of particle transport in phase space. The grey color indicates the parametric area of the expected phase space density depletion: particles are scattered from this region to smaller energy/pitch-angle whereas particle scattered into this region come from a lower phase space density region. Black color indicates the areas of the expected phase space density increase: particles are scattered (to lower energies) or transported by trapping (to higher energies) into these regions. Two red arrows connecting these different areas show that trapping acceleration is not a local process.



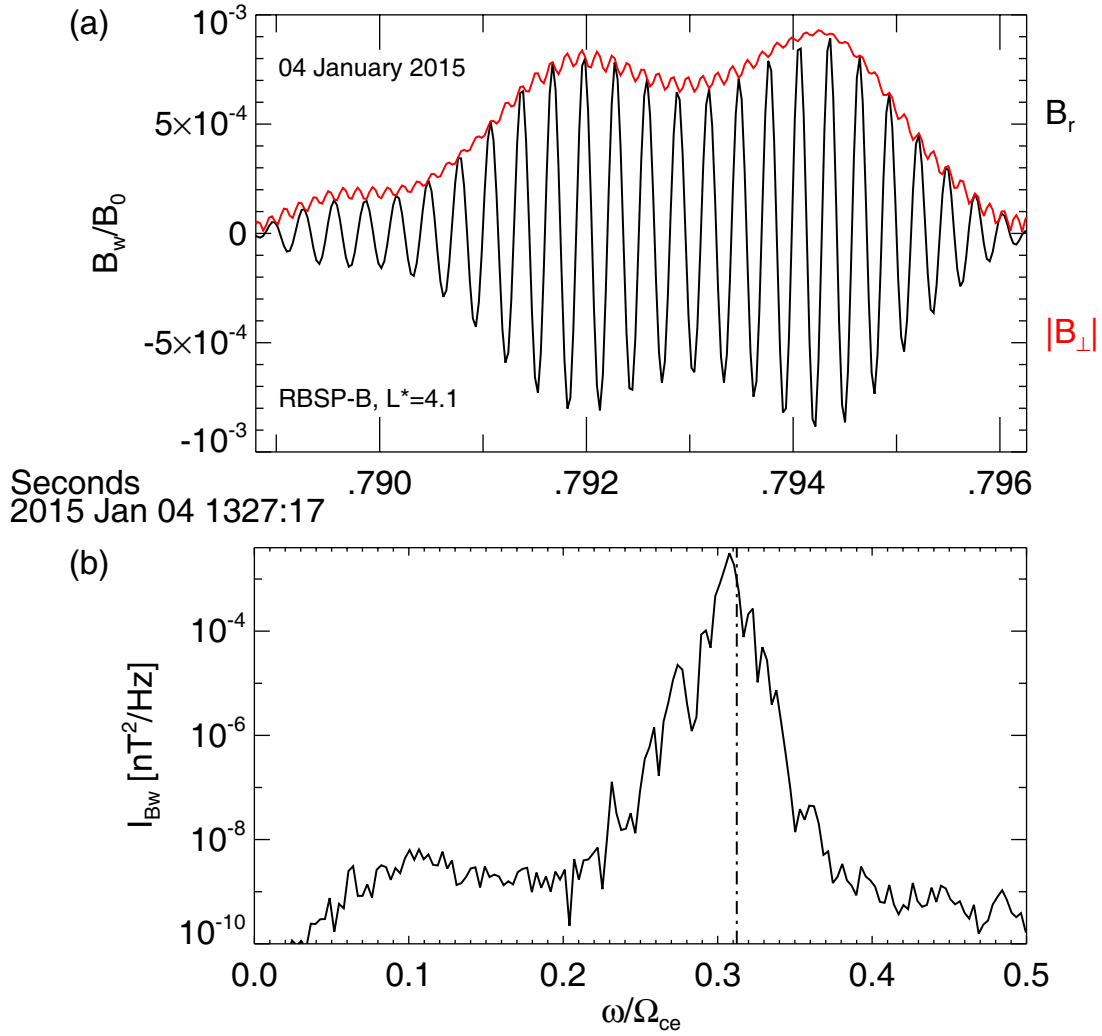


**Figure 2.** Example of long wave-packets, wave-packet,  $B_\perp$  and  $B_\perp/B_0$ , spectrum with  $\omega/\Omega_{ce}$ .

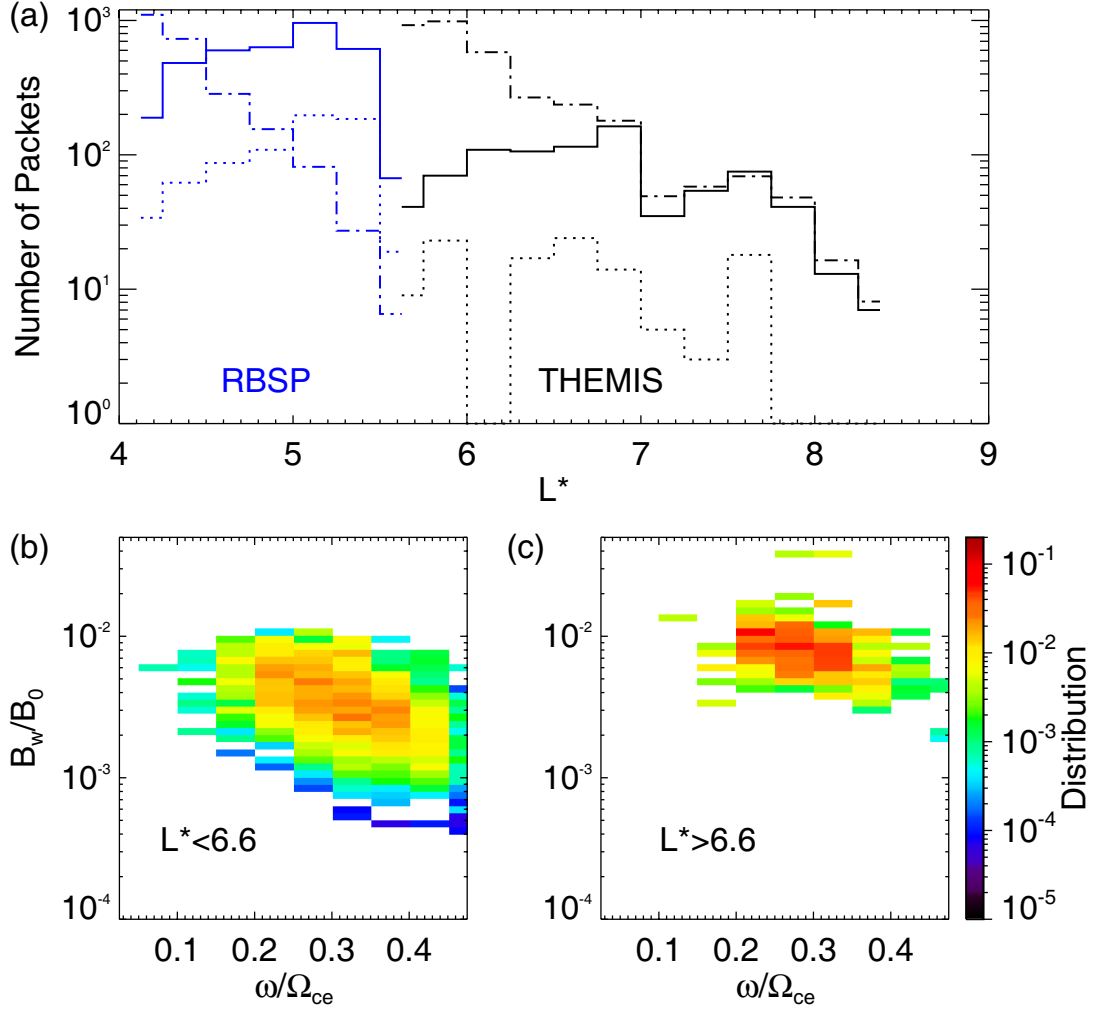


**Figure 3.** (a) Per day observations of wave-packets of intense chorus wave as a function of  $L^*$  for  $\beta > 50$  (solid lines) and  $\beta^* > 50$  (dotted lines), (b), (c) distributions in  $B_w, \omega/\Omega_{ce}(0)$  for  $\mathcal{B}_w > 2$  and  $\beta > 50$ , for two  $L^*$ -shell ranges.

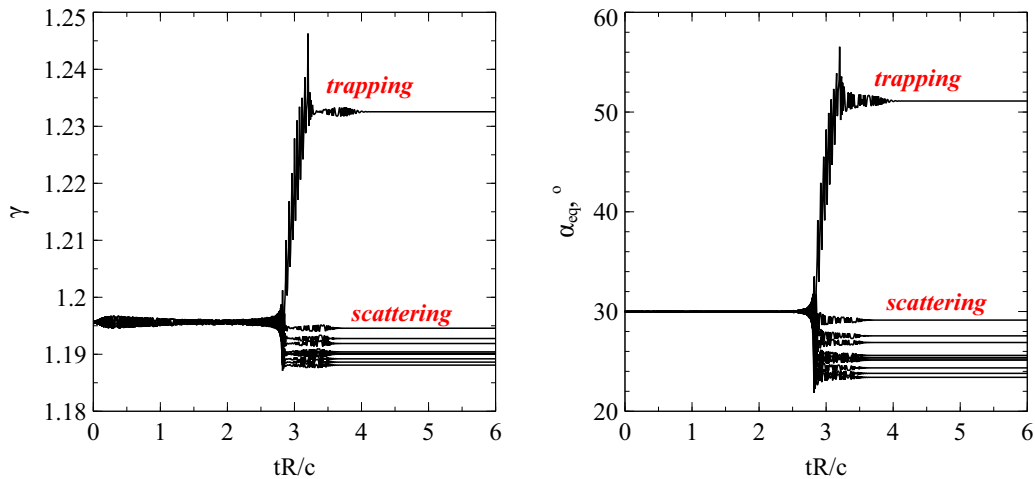


**Figure 4.** Results of numerical integration of 10 particle trajectories described by Eqs. (3). All particles have the same initial energy and equatorial pitch-angle (initial  $I_x$ ), and different (randomly distributed) initial phases  $\psi$ . Panels show energy (left panel) and equatorial pitch-angle (right panel) as a function of dimensionless time (trajectories are integrated for  $\sim$  a quarter of the bounce period; there is only one resonance for each trajectory). System parameters are:  $L = 6$ ,  $\omega/\Omega_{ce}(0) = 0.35$ ,  $B_w = 500\text{pT} \cdot \tanh(\lambda/5^\circ) \exp -(\lambda/25^\circ)^2$  for  $\lambda > 0$  [i.e., the latitudinal distribution used the mimics observed wave field distribution, see *Agapitov et al.*, 2013].

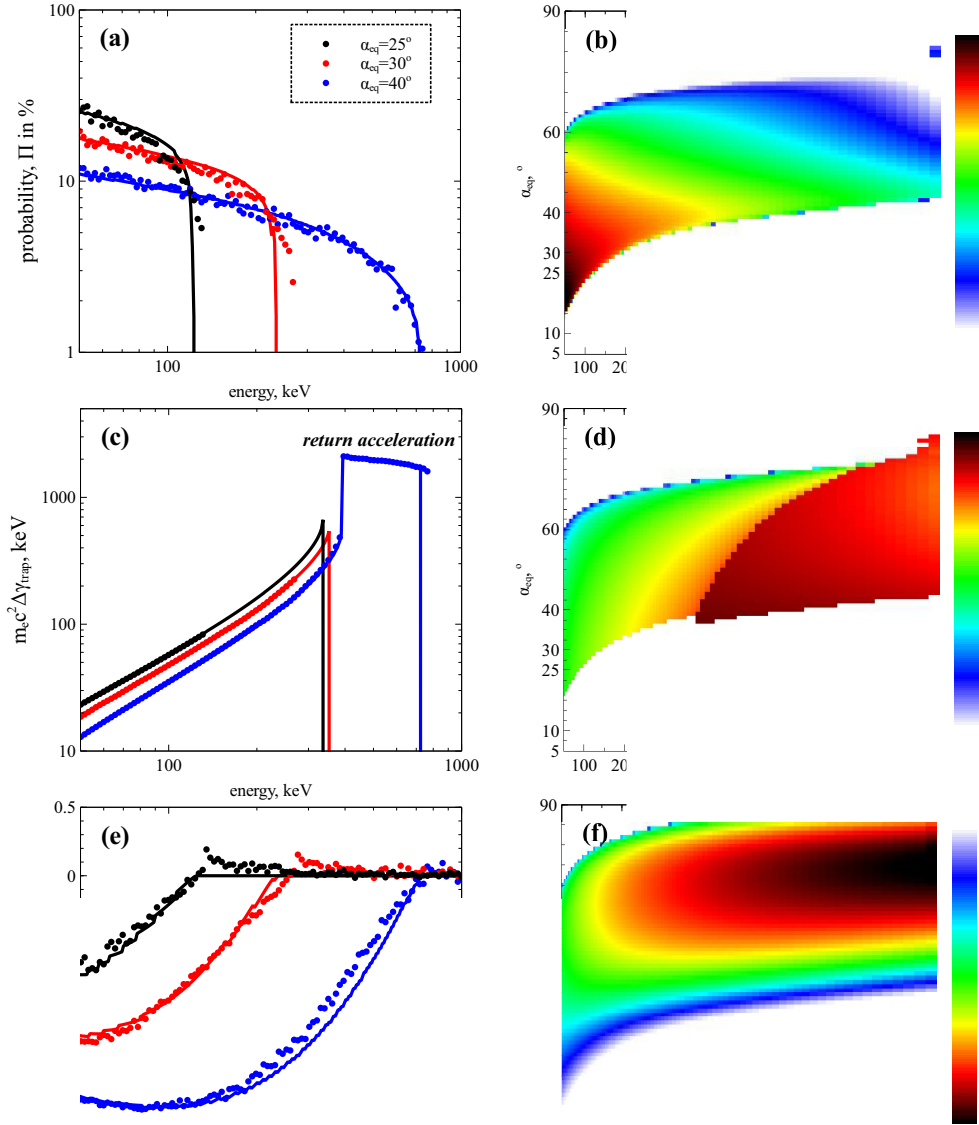


**Figure 5.** Panels (a), (c), and (e): Probability of trapping, energy change of trapped particles, and energy change of nonlinearly scattered particles as functions of particle initial energy for three initial pitch-angles. Curves are analytical results and circles are results of numerical integration of Hamiltonian equations (3); each circle representing values averaged over 5000 trajectories. Panels (b), (d), and (f): Analytically evaluated probability of trapping, energy change of trapped particles, and energy change of scattered particles. System parameters are the same as in Fig. 4. In panels (c) and (d) we indicate

the parameter region of the turning acceleration characterized by a more significant energy gain [see details in *Omura et al.*, 2007].

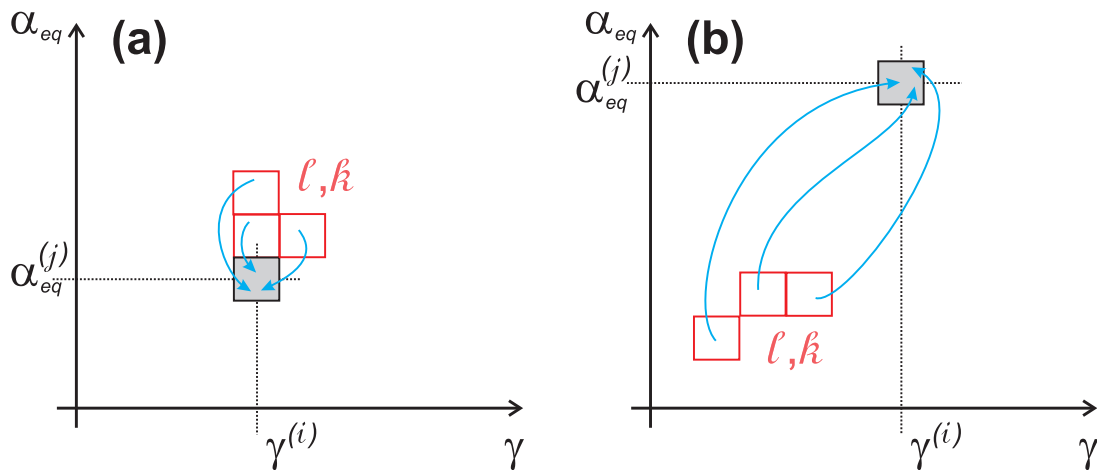


**Figure 6.** Schematic view of operators describing (local) nonlinear scattering (a) and (nonlocal) trapping (b) in the energy/pitch-angle space. Red cells form the sets of  $(k, l)$  indexes for scattered and trapped particles.

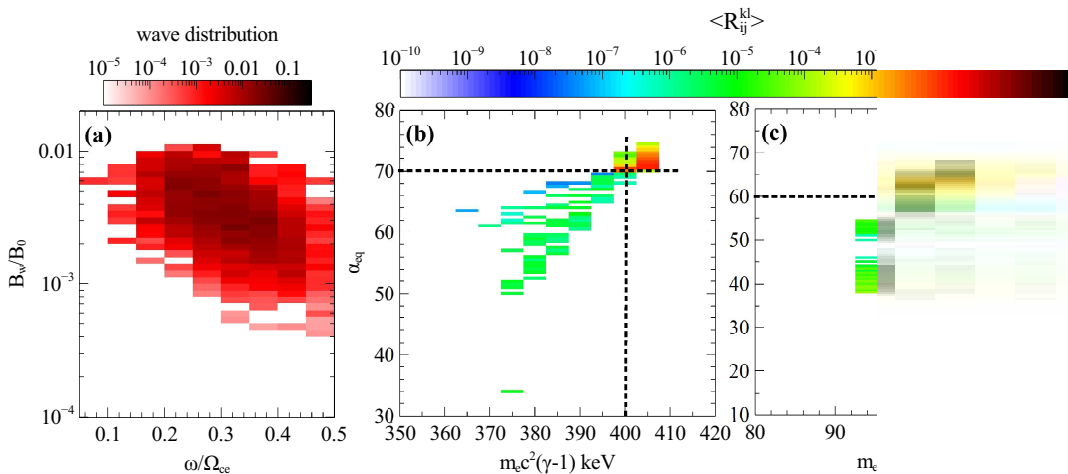


**Figure 7.** (a) A model wave distribution in the  $(B_w, \omega/\Omega_{ce})$  space (taken from Fig. 3 for  $L^* < 6.6$ ). (b) and (c): Two functions  $\langle R_{ij}^{kl} \rangle$  plotted for two *target* cells:  $(m_e c^2(\gamma^{(i)} - 1) = 400\text{keV}, \alpha_{eq}^{(j)} = 70^\circ)$  (b) and  $(m_e c^2(\gamma^{(i)} - 1) = 100\text{keV}, \alpha_{eq}^{(j)} = 60^\circ)$  (c). Black lines in panels (b), (c) cross at the *target* cells.

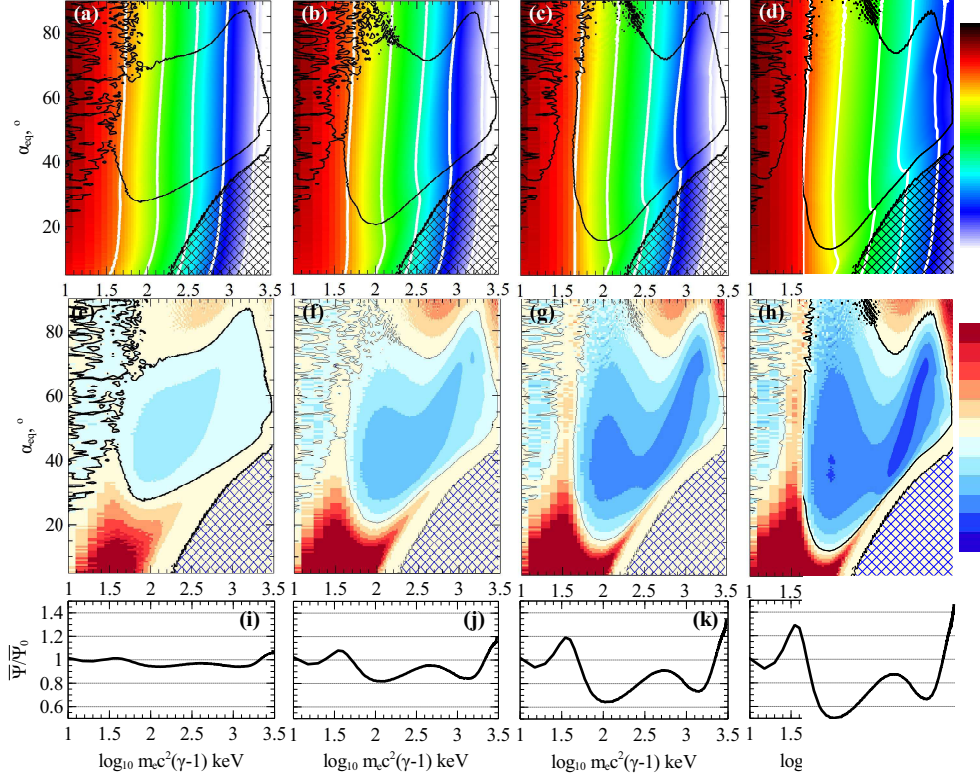


**Figure 8.** Evolution of the electron distribution function due to nonlinear interactions with intense chorus waves. Panels (a)-(d) show the solution of Eq. (11) for an initial distribution  $\Psi_0 = (1 + (\gamma - 1)/c_\kappa)^{-\kappa-1} \sin \alpha_{eq}$  with  $c_\kappa = (\kappa - 3/2)/50$  and  $\kappa = 4$ . The results of numerical calculations are displayed at times  $\tau = 10$  (a),  $\tau = 30$  (b),  $\tau = 60$  (c), and  $\tau = 100$  (d). Panels (e)-(h) show the ratio of distributions from panels (a)-(d) over the initial distribution. Panels (i)-(l) show the integrated distributions  $\bar{\Psi} = \int \Psi \sin \alpha_{eq} d\alpha_{eq}$  normalized to the initial integrated distribution  $\bar{\Psi}_0$ . Shaded domains in panels (a)-(h) show the parameter domains of non-resonant particles. Solid black curves in panels (a)-(h) correspond to  $\Psi/\Psi_0 = 1$ .

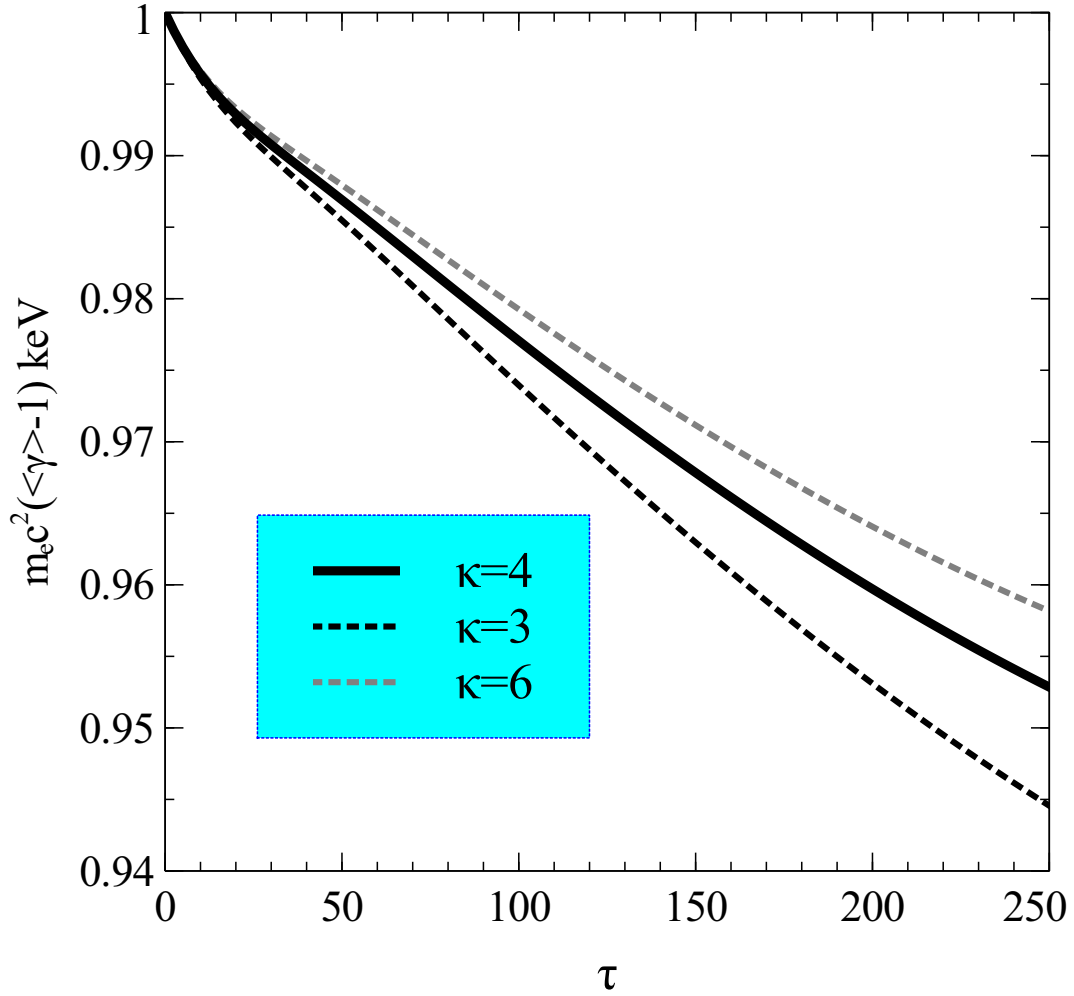


**Figure 9.** Left panel: evolution of the total particle energy for initial distributions  $\Psi_0 = (1 + (\gamma - 1)/c_\kappa)^{-\kappa-1} \sin \alpha_{eq}$  with  $c_\kappa = (\kappa - 3/2)/50$  and three values of  $\kappa$ . Right panel: Evolution of total particle energy for initial distributions  $\Psi_0 = (1 + (\gamma - 1)/c_\kappa)^{-\kappa-1} G(\alpha_{eq})$  with four different  $G(\alpha_{eq})$  functions;  $c_\kappa = (\kappa - 3/2)/50$  and  $\kappa = 4$ .

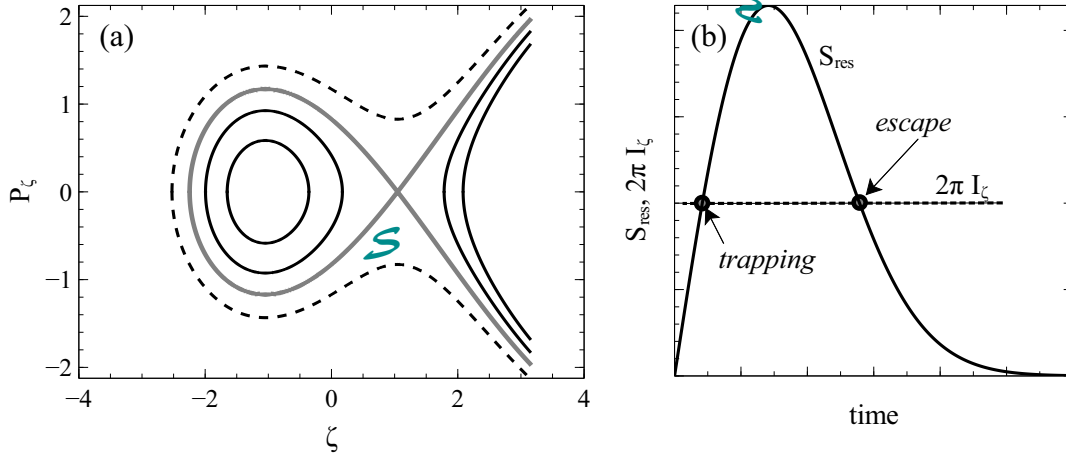


**Figure 10.** (a) Phase portrait of Hamiltonian  $H_\zeta$  given by Eq. (18). Grey color shows the separatrix, closed solid curves are trajectories of trapped particles, the dotted curve is the trajectory of a transient (scattered) particle. (b) A schematic view of the determination of trapping and escaping times. (c) Results of numerical integration of Hamiltonian equations and analytical expressions (16), (20); see details in the text. (d) A fragment of trapped particle trajectory in the  $(\zeta, P_\zeta)$  plane; dimensionless parameter  $\chi = \Omega_{ce}(0)R_EL/c$ . System parameters are the same as in Fig. 4.